

1           Quasi-consistent efficient meshfree thin shell  
2       formulation ~~to-with~~ naturally ~~accommodate stabilized~~  
3       essential boundary ~~conditions~~~~condition enforcement~~

4           Junchao Wu<sup>a,\*</sup>, Yangtao Xu<sup>a</sup>, Bin Xu<sup>a</sup>, Syed Humayun Basha<sup>a</sup>

<sup>a</sup>*Key Laboratory for Intelligent Infrastructure and Monitoring of Fujian Province, Key Laboratory for Structural Engineering and Disaster Prevention of Fujian Province, College of Civil Engineering, Huaqiao University, Xiamen, Fujian, 361021, China*

---

5           **Abstract**

This research proposed an efficient and quasi-consistent meshfree thin shell formulation with ~~natural~~ ~~naturally stabilized~~ enforcement of essential boundary conditions. Within the framework of the Hu-Washizu variational principle, a mixed formulation of displacements, strains and stresses is employed in this approach, where the displacements are discretized using meshfree shape functions, and the strains and stresses are expressed using smoothed gradients, covariant smoothed gradients and covariant bases. The smoothed gradients satisfy the first ~~and second order~~ ~~second-order~~ integration constraint and have ~~quasi-consistent consistency~~ ~~variational consistency for polynomial strains and stresses~~. Owing to Hu-Washizu variational principle, the essential boundary conditions automatically arise in its weak form. As a result, the suggested technique's enforcement of essential boundary conditions resembles that of the traditional Nitsche's method. Contrary to Nitsche's method, the costly higher order derivatives of conventional meshfree shape functions were replaced by the smoothed gradients with fast computation, which improve the efficiency. Meanwhile, the proposed formulation features a naturally stabilized term without adding any artificial stabilization factors, which eliminates the ~~stabilization parameter-dependent issue in the Nitsche's method~~ ~~employment of penalty method as a stabilization~~. The efficacy of the proposed Hu-Washizu meshfree thin shell formulation is illustrated by a set of classical standard thin shell problems.

6           *Keywords:* Meshfree, Thin shell, Hu-Washizu variational principle,  
7       Reproducing kernel gradient smoothing, Essential boundary condition

---

---

\*Corresponding author  
Email address: [jcwu@hqu.edu.cn](mailto:jcwu@hqu.edu.cn) (Junchao Wu)

8      **1. Introduction**

9      Thin shell structures generally adhere to the Kirchhoff hypothesis [1], that  
10     neglects the shear deformation can be described using Galerkin formulation  
11     which requires to have at least  $C^1$  continuity. The traditional finite element  
12     methods usually ~~only~~ have  $C^0$  continuous shape functions, and it prefers Mindlin  
13     thick shear theory, hybrid and mixed models in simulation of shell structure [2].  
14     Meshfree methods [3, 4, 5] with high order smoothed shape functions have gar-  
15     nered much research attention over the past thirty years. These techniques  
16     established the shape functions based on a collection of dispersed nodes, and  
17     ~~the~~-high order continuity of shape functions can be easily achieved even with  
18     low-order basis functions. For thin shell analysis, ~~this~~-high order meshfree ap-  
19     proximation can also ~~further~~ alleviate the membrane locking caused by the  
20     mismatched approximation order of membrane strain and bending strain [6].  
21     ~~Furthermore~~Moreover, nodal-based meshfree approximations generally offer the  
22     flexibility of local refinement and can relieve the burden of mesh distortion.  
23     Owing to these benefits, numerous meshfree techniques have been developed  
24     and implemented in many scientific and engineering fields ~~[7, 8, 9, 10, 11, 12]~~  
25     [7, 8, 9, 10, 11, 12, 13]. However, the high order smoothed meshfree shape func-  
26     tions accompany the enlarged and overlapping supports, which may potentially  
27     cause many problems for shape functions. One of the issues is the loss of the  
28     Kronecker delta property, which means that, unlike the finite element methods,  
29     the necessary boundary conditions cannot be directly enforced [14]. Another  
30     issue is that the variational consistency or said integration constraint, which  
31     is a condition that requires the formulation to exactly reproduce the solution  
32     spanned by the basis functions, cannot be satisfied~~due to~~. This issue is mainly  
33     caused by the misalignment between the numerical integration domains and sup-  
34     ports of shape functions. ~~Besides~~Thus, the shape functions exhibit a piecewise  
35     rational-nature in each integration domain. ~~Besides, it has to be noted that the~~  
36     traditional integration rules like Gauss scheme cannot ensure the integration  
37     accuracy in Galerkin weak form [15, 16]. Therefore, variational consistency  
38     is vital to the solution accuracy in ~~Galerkin formulations [15, 16]~~the Galerkin  
39     meshfree formulations.

40     Various ways have been presented to enforce the necessary boundary for  
41     Galerkin meshfree methods directly, including the boundary singular kernel  
42     method [17], mixed transformation method [17], and interpolation element-free  
43     method [18] for recovering shape functions' Kronecker property. However, these  
44     methods are not based on a variational setting and cannot guarantee varia-  
45     tional consistency. In the absence of a meshfree node, accuracy enforcement  
46     might be ~~poorer~~poor. In contrast, enforcing the essential boundary conditions  
47     using a variational approach is preferred for Galerkin meshfree methods. The  
48     variational consistent Lagrange multiplier approach was initially used to the  
49     Galerkin meshfree method by Belytschko et al. [3]. In this method, the extra  
50     degrees of freedom are used to determine the discretion of Lagrange multiplier.  
51     Furthermore, Ivannikov et al. [19] have extended this approach to geometri-  
52     cally nonlinear thin shells. Lu et al. [20] suggested the modified variational es-

53 essential boundary enforcement approach and expressed the Lagrange multiplier  
54 by equivalent tractions to eliminate the excess degrees of freedom. However,  
55 the coercivity of this approach is not always ensured and potentially reduces  
56 the accuracy. Zhu and Atluri [21] pioneered the penalty method for meshfree  
57 method, making it a straightforward approach to enforce essential boundary  
58 conditions via Galerkin weak form. However, the penalty method lacks varia-  
59 tional consistency and requires experimental artificial parameters whose optimal  
60 value is hard to determine. Fernández-Méndez and Huerta [14] imposed neces-  
61 sary boundary conditions using Nitsche’s approach in the meshfree formulation.  
62 This approach can be seen as a hybrid combination of the modified variational  
63 method and the penalty method because the modified variational method gen-  
64 erates variational consistency through the use of a consistent term, and the  
65 penalty method is used as a stabilized term to recover the coercivity. Skatulla  
66 and Sansour [22] extended Nitsche’s thin shell analysis method and proposed an  
67 iteration algorithm to determine artificial parameters at each integration point.

68 In order to address the issue of numerical integration, a series of consis-  
69 tent integration schemes have been developed for Galerkin meshfree methods.  
70 Among these include stabilized conforming nodal integration [23], variational  
71 consistent integration [24], quadratic consistent integration [25], reproducing  
72 kernel gradient smoothing integration [26], and consistent projection integration  
73 [27]. The assumed strain approach establishes the most consistent integration  
74 scheme, while the smoothed gradient replaces the costly higher order derivatives  
75 of traditional meshfree shape functions and shows a high efficiency. Moreover,  
76 to achieve global variational consistency, a consistent essential boundary con-  
77 dition enforcement should cooperate with the consistent integration scheme.  
78 The consistent integration scheme and Nitsche’s method for treating essential  
79 boundary conditions show a good performance since they can satisfy the coer-  
80 civity without requiring additional degrees of freedom. Nevertheless, Nitsche’s  
81 approach still retains the artificial parameters in stabilized terms, and it is es-  
82 sential to remain conscious of the costly higher order derivatives, particularly  
83 for thin plate and thin shell problems. Recently, Wu et al. [28, 29] proposed  
84 an efficient and stabilized essential boundary condition enforcement method  
85 based upon the Hellinger-Reissner variational principle, where a mixed formu-  
86 lation in Hellinger-Reissner weak form recasts the reproducing kernel gradient  
87 smoothing integration. The terms for enforcing essential boundary conditions  
88 are identical to the Nitsche’s method, and both have consistent and stabilized  
89 terms. Nevertheless, the stabilized term of this method naturally exists in the  
90 Hellinger-Reissner weak form and no longer needs the artificial parameters, even  
91 for essential boundary enforcement; instead all of the higher order derivatives  
92 are represented by smoothed gradients and their derivatives.

93 In this study, an efficient and stabilized variational consistent meshfree  
94 method that naturally enforces the essential boundary conditions is developed  
95 for thin shell structure. Following the concept of the Hellinger-Reissner prin-  
96 ciple base consistent meshfree method, the Hu-Washizu variational principle of  
97 complementary energy with variables of displacement, strains, and stresses is  
98 employed. The displacement is approximated by conventional meshfree shape

99 functions, and the strains and stresses are expressed by smoothed gradients with  
100 covariant bases. It is important to note that although the first second-order in-  
101 tegration requirements are naturally embedded in the smoothed gradients, their  
102 fulfillment can only result in a quasi-satisfaction of variational consistency be-  
103 cause of the non-polynomial nature of the stresses. Hu-Washizu's weak form is  
104 used to evaluate all the essential boundary conditions regarding displacements  
105 and rotations. This type of formulation is similar to the Nitsche's method but  
106 does not require any artificial parameters. Compared with Nitsche's method,  
107 conventional reproducing smoothed gradients and its direct derivatives replace  
108 the costly higher order derivatives. By utilizing the advantages of a replicating  
109 kernel gradient smoothing framework, the smoothed gradients showed better  
110 performance compared to conventional derivatives of shape functions, hence  
111 increasing the meshfree formulation's computational efficiency.

112 The remainder of this research paper is structured as follows: The kinematics  
113 of the thin shell structure and the weak form of the associated Hu-Washizu  
114 principle are briefly described in Section 2. Subsequently, the mixed formulation  
115 regarding the displacements, strains and stresses in accordance with Hu-Washizu  
116 weak form are presented in Section 3. The discrete equilibrium equations are  
117 derived in Section 4 using the naturally occurring accommodation of essential,  
118 and they are compared to the equations obtained using Nitsche's method. The  
119 numerical results in Section 5 validate the efficacy of the proposed Hu-Washizu  
120 meshfree thin shell formulation. Lastly, the concluding remarks are presented  
121 in Section 6.

<sup>122</sup> **2. Hu-Washizu's formulation of complementary energy for thin shell**

<sup>123</sup> *2.1. Kinematics for thin shell*

<sup>124</sup> Consider the configuration of a shell  $\bar{\Omega}$ , as shown in Fig. 1, which can be  
<sup>125</sup> easily described by a parametric curvilinear coordinate system  $\xi = \{\xi^i\}_{i=1,2,3}$ .  
<sup>126</sup> The mid-surface of the shell denoted by  $\Omega$  is specified by the in-plane coordinates  
<sup>127</sup>  $\xi = \{\xi^\alpha\}_{\alpha=1,2}$ , as the thickness direction of shell is by  $\xi^3$ ,  $-\frac{h}{2} \leq \xi^3 \leq \frac{h}{2}$ ,  $h$  is  
<sup>128</sup> the thickness of shell. In this work, Latin indices take the values from 1 to 3,  
<sup>129</sup> and Greek indices are evaluated by 1 or 2. For the Kirchhoff hypothesis [6], the  
<sup>130</sup> position  $\mathbf{x} \in \bar{\Omega}$  is defined by linear functions with respect to  $\xi^3$  :

$$\mathbf{x}(\xi^1, \xi^2, \xi^3) = \mathbf{r}(\xi^1, \xi^2) + \xi^3 \mathbf{a}_3(\xi^1, \xi^2) \quad (1)$$

in which  $\mathbf{r}$  means the position on the mid-surface of shell, and  $\mathbf{a}_3$  is correspond-

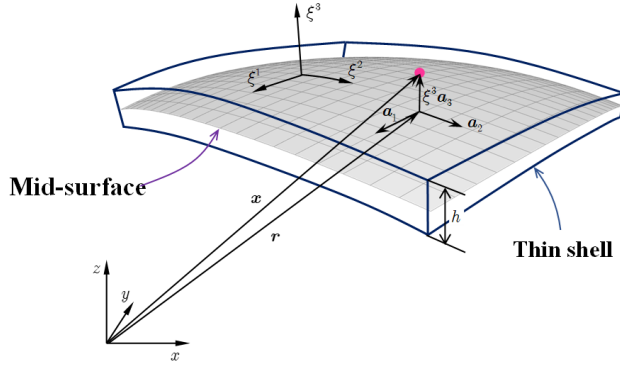


Figure 1: Kinematics for thin shell.

<sup>131</sup>  
<sup>132</sup> ing normal direction. For the mid-surface of shell, the in-plane covariant base  
<sup>133</sup> vector with respect to  $\xi^\alpha$  can be derived by a trivial partial differentiation to  $\mathbf{r}$ :

$$\mathbf{a}_\alpha = \frac{\partial \mathbf{r}}{\partial \xi^\alpha} = \mathbf{r}_{,\alpha}, \alpha = 1, 2 \quad (2)$$

<sup>134</sup> to provide for a clear expression, the subscript comma denotes the partial dif-  
<sup>135</sup> ferentiation operation with respect to in-plane coordinates  $\xi^\alpha$ , and the normal  
<sup>136</sup> vector  $\mathbf{a}_3$  can be obtained by the normalized cross product of  $\mathbf{a}_\alpha$ 's as follows:

$$\mathbf{a}_3 = \frac{\mathbf{a}_1 \times \mathbf{a}_2}{\|\mathbf{a}_1 \times \mathbf{a}_2\|} \quad (3)$$

<sup>137</sup> where  $\|\bullet\|$  is the Euclidean norm operator.

<sup>138</sup> With the assumption of infinitesimal deformation, the strain components  
<sup>139</sup> with respect to the global contravariant base can be stated as:

$$\epsilon_{ij} = \frac{1}{2} (\mathbf{x}_{,i} \cdot \mathbf{u}_{,j} + \mathbf{u}_{,i} \cdot \mathbf{x}_{,j}) \quad (4)$$

<sup>140</sup> where  $\mathbf{u}$  represents the displacement for the shell deformation. To satisfy the  
<sup>141</sup> Kirchhoff hypothesis, the displacement is assumed to be of the following form:

$$\mathbf{u}(\xi^1, \xi^2, \xi^3) = \mathbf{v}(\xi^1, \xi^2) + \boldsymbol{\theta}(\xi^1, \xi^2)\xi^3 \quad (5)$$

<sup>142</sup> in which the quadratic and higher order terms are neglected.  $\mathbf{v}, \boldsymbol{\theta}$  represent  
<sup>143</sup> the displacement and rotation in mid-surface, respectively.

<sup>144</sup> Subsequently, plugging Eqs. (1) and (5) into Eq. (4) and neglecting the  
<sup>145</sup> quadratic terms, the strain components can be rephrased as follows:

$$\begin{aligned} \epsilon_{\alpha\beta} &= \frac{1}{2}(\mathbf{a}_\alpha \cdot \mathbf{v}_{,\beta} + \mathbf{v}_{,\alpha} \cdot \mathbf{a}_\beta) \\ &+ \frac{1}{2}(\mathbf{a}_{3,\alpha} \cdot \mathbf{v}_{,\beta} + \mathbf{v}_{,\alpha} \cdot \mathbf{a}_{3,\beta} + \mathbf{a}_\alpha \cdot \boldsymbol{\theta}_{,\beta} + \boldsymbol{\theta}_{,\alpha} \cdot \mathbf{a}_\beta)\xi^3 \end{aligned} \quad (6a)$$

$$\epsilon_{\alpha 3} = \frac{1}{2}(\mathbf{a}_\alpha \cdot \boldsymbol{\theta} + \mathbf{v}_{,\alpha} \cdot \mathbf{a}_3) + \frac{1}{2}(\mathbf{a}_3 \cdot \boldsymbol{\theta})_{,\alpha}\xi^3 \quad (6b)$$

$$\epsilon_{33} = \mathbf{a}_3 \cdot \boldsymbol{\theta} \quad (6c)$$

<sup>146</sup> where  $\epsilon_{\alpha\beta}, \kappa_{\alpha\beta}$  represent membrane and bending strains, respectively, and are  
<sup>147</sup> given as follows:

$$\epsilon_{\alpha\beta} = \frac{1}{2}(\mathbf{a}_\alpha \cdot \mathbf{v}_{,\beta} + \mathbf{v}_{,\alpha} \cdot \mathbf{a}_\beta) \quad (7)$$

$$\kappa_{\alpha\beta} = \frac{1}{2}(\mathbf{a}_{3,\alpha} \cdot \mathbf{v}_{,\beta} + \mathbf{v}_{,\alpha} \cdot \mathbf{a}_{3,\beta} + \mathbf{a}_\alpha \cdot \boldsymbol{\theta}_{,\beta} + \boldsymbol{\theta}_{,\alpha} \cdot \mathbf{a}_\beta) \quad (8)$$

<sup>149</sup> In accordance with the Kirchhoff hypothesis, the thickness of shell will not  
<sup>150</sup> change, and the deformation related with direction of  $\xi^3$  will vanish, i.e.  $\epsilon_{3i} = 0$ .  
<sup>151</sup> Thus, the rotation  $\boldsymbol{\theta}$  can be rewritten as:

$$\epsilon_{3i} = 0 \Rightarrow \begin{cases} \boldsymbol{\theta} \cdot \mathbf{a}_\alpha \cancel{=} -\mathbf{v}_{,\alpha} \cdot \mathbf{a}_3 \cancel{=} 0 \\ \boldsymbol{\theta} \cdot \mathbf{a}_3 = 0 \end{cases} \Rightarrow \boldsymbol{\theta} = -\mathbf{v}_{,\alpha} \cdot \mathbf{a}_3 \mathbf{a}^\alpha \quad (9)$$

<sup>152</sup> where  $\mathbf{a}^\alpha$ 's is the in-plane contravariant base vector,  $\mathbf{a}^\alpha \cdot \mathbf{a}_\beta = \delta_\beta^\alpha$ ,  $\delta$  is the  
<sup>153</sup> Kronecker delta function. Substituting Eq. The detailed derivation of Eq. 9  
<sup>154</sup> can be found in reference [31].

<sup>155</sup> Furthermore, substituting Eq. (9) into Eq. (8) leads to:

$$\kappa_{\alpha\beta} = (\Gamma_{\alpha\beta}^\gamma \mathbf{v}_{,\gamma} - \mathbf{v}_{,\alpha\beta}) \cdot \mathbf{a}_3 = -\mathbf{v}_{,\alpha}|_\beta \cdot \mathbf{a}_3 \quad (10)$$

<sup>156</sup> in which  $\Gamma_{\alpha\beta}^\gamma = \mathbf{a}_{\alpha,\beta} \cdot \mathbf{a}^\gamma$  is namely the Christoffel symbol of the second kind, and  
<sup>157</sup>  $\mathbf{v}_{,\alpha}|_\beta$  is the in-plane covariant derivative of  $\mathbf{v}_{,\alpha}$ , i.e.  $\mathbf{v}_{,\alpha}|_\beta = \Gamma_{\alpha\beta}^\gamma \mathbf{v}_{,\gamma} - \mathbf{v}_{,\alpha\beta}$ .

## <sup>158</sup> 2.2. Galerkin weak form for Hu-Washizu principle of complementary energy

<sup>159</sup> In this study, the Hu-Washizu variational principle of complementary energy  
<sup>160</sup> [32] was adopted for the development of the proposed analytical approach, the

<sup>161</sup> corresponding complementary functional, denoted by  $\Pi_C$ , is listed as follows:

$$\begin{aligned} & \Pi_C(\varepsilon_{\alpha\beta}, \kappa_{\alpha\beta}, N^{\alpha\beta}, M^{\alpha\beta}) \\ &= \int_{\Omega} \frac{h}{2} \varepsilon_{\alpha\beta} C^{\alpha\beta\gamma\eta} \varepsilon_{\gamma\eta} d\Omega + \int_{\Omega} \frac{h^3}{24} \kappa_{\alpha\beta} C^{\alpha\beta\gamma\eta} \kappa_{\gamma\eta} d\Omega \\ &+ \int_{\Omega} \varepsilon_{\alpha\beta} (N^{\alpha\beta} - h C^{\alpha\beta\gamma\eta} \varepsilon_{\gamma\eta}) d\Omega + \int_{\Omega} \kappa_{\alpha\beta} (M^{\alpha\beta} - \frac{h^3}{12} C^{\alpha\beta\gamma\eta} \kappa_{\gamma\eta}) d\Omega \\ &- \int_{\Gamma_v} \mathbf{T} \cdot \bar{\mathbf{v}} d\Gamma + \int_{\Gamma_\theta} M_{\mathbf{n}\mathbf{n}} \bar{\theta}_{\mathbf{n}} d\Gamma - (P \mathbf{a}_3 \cdot \bar{\mathbf{v}})_{\mathbf{x} \in C_w} \end{aligned} \quad (11)$$

<sup>162</sup> where  $C^{\alpha\beta\gamma\eta}$ 's represent the components of fourth order elasticity tensor with  
<sup>163</sup> respect to the covariant base and plane stress assumption, and it can be ex-  
<sup>164</sup> pressed by Young's modulus  $E$ , Poisson's ratio  $\nu$  and the in-plane contravariant  
<sup>165</sup> metric coefficients  $a^{\alpha\beta}$ 's,  $a^{\alpha\beta} = \mathbf{a}^\alpha \cdot \mathbf{a}^\beta$ , as follows:

$$C^{\alpha\beta\gamma\eta} = \frac{E}{2(1+\nu)} (a^{\alpha\gamma} a^{\beta\eta} + a^{\alpha\eta} a^{\beta\gamma} + \frac{2\nu}{1-\nu} a^{\alpha\beta} a^{\gamma\eta}) \quad (12)$$

<sup>166</sup> and  $N^{\alpha\beta}$ ,  $M^{\alpha\beta}$  are the components of membrane and bending stresses given by:

$$N^{\alpha\beta} = h C^{\alpha\beta\gamma\eta} \varepsilon_{\gamma\eta}, \quad M^{\alpha\beta} = \frac{h^3}{12} C^{\alpha\beta\gamma\eta} \kappa_{\gamma\eta} \quad (13)$$

<sup>167</sup> Essential boundaries on the edges and corners denoted by  $\Gamma_v$ ,  $\Gamma_\theta$  and  $C_v$  are  
<sup>168</sup> naturally existed in complementary energy functional,  $\bar{\mathbf{v}}$ ,  $\bar{\theta}_{\mathbf{n}}$  are the correspond-  
<sup>169</sup> ing prescribed displacement and normal rotation, respectively.  $\mathbf{T}$ ,  $M_{\mathbf{n}\mathbf{n}}$  and  $P$   
<sup>170</sup> can be determined by Euler-Lagrange equations of shell problem [31] as follows:

$$\mathbf{T} = \mathbf{T}_N + \mathbf{T}_M \rightarrow \begin{cases} \mathbf{T}_N = \mathbf{a}_\alpha N^{\alpha\beta} n_\beta \\ \mathbf{T}_M = (\mathbf{a}_3 M^{\alpha\beta} s_\alpha n_\beta)_{,\gamma} s^\gamma + (\mathbf{a}_3 M^{\alpha\beta})|_\beta n_\alpha \end{cases} \quad (14)$$

$$M_{\mathbf{n}\mathbf{n}} = M^{\alpha\beta} n_\alpha n_\beta \quad (15)$$

$$P = -[[M^{\alpha\beta} s_\alpha n_\beta]] \quad (16)$$

<sup>173</sup> where  $\mathbf{n} = n^\alpha \mathbf{a}_\alpha = n_\alpha \mathbf{a}^\alpha$  and  $\mathbf{s} = s^\alpha \mathbf{a}_\alpha = s_\alpha \mathbf{a}^\alpha$  are the outward normal and  
<sup>174</sup> tangent directions on boundaries.  $[[f]]$  is the jump operator defined by:

$$[[f]]_{\mathbf{x}=\mathbf{x}_c} = \lim_{\epsilon \rightarrow 0^+} (f(\mathbf{x}_c + \epsilon) - f(\mathbf{x}_c - \epsilon)), \mathbf{x}_c \in \Gamma \quad (17)$$

<sup>175</sup> where  $f$  is an arbitrary function on  $\Gamma$ .

<sup>176</sup> Moreover, the natural boundary conditions should be applied by Lagrangian  
<sup>177</sup> multiplier method with displacement  $\mathbf{v}$  regarded as multiplier. Thus, then the  
<sup>178</sup> new complementary energy functional namely  $\Pi$  is given by:

$$\begin{aligned} & \Pi(\mathbf{v}, \varepsilon_{\alpha\beta}, \kappa_{\alpha\beta}, N^{\alpha\beta}, M^{\alpha\beta}) \\ &= \Pi_C(\varepsilon_{\alpha\beta}, \kappa_{\alpha\beta}, N^{\alpha\beta}, M^{\alpha\beta}) + \int_{\Gamma_M} \bar{\theta}_{\mathbf{n}} (M_{\mathbf{n}\mathbf{n}} - \bar{M}_{\mathbf{n}\mathbf{n}}) d\Gamma \\ &- \int_{\Gamma_T} \mathbf{v} \cdot (\mathbf{T} - \bar{\mathbf{T}}) d\Gamma - \mathbf{v} \cdot \mathbf{a}_3 (P - \bar{P})_{\mathbf{x} \in C_P} - \int_{\Omega} \mathbf{v} \cdot (\mathbf{b} - \bar{\mathbf{b}}) d\Omega \end{aligned} \quad (18)$$

179 where  $\bar{\mathbf{T}}$ ,  $\bar{\mathbf{M}}_{nn}$ ,  $\bar{\mathbf{M}}_{nn}$  and  $\bar{P}$  are the prescribed traction, bending moment and  
 180 concentrated force on edges  $\Gamma_T$ ,  $\Gamma_M$  and corner  $C_P$  respectively. All the bound-  
 181aries meet the following geometric relationships:

$$\begin{cases} \Gamma = \Gamma_v \cup \Gamma_T \cup \Gamma_\theta \cup \Gamma_M, & C = C_v \cup C_P, \\ \Gamma_v \cap \Gamma_T = \Gamma_\theta \cap \Gamma_M = C_v \cap C_P = \emptyset \end{cases} \quad (19)$$

182 and  $\bar{\mathbf{b}}$  stands for the prescribed body force in  $\Omega$ ,  $\mathbf{b}$  also can be written based on  
 183 Euler-Lagrange equations [31] as:

$$\mathbf{b} = \mathbf{b}_N + \mathbf{b}_M \rightarrow \begin{cases} \mathbf{b}_N = (\mathbf{a}_\alpha N^{\alpha\beta})|_\beta \\ \mathbf{b}_M = (\mathbf{a}_3 M^{\alpha\beta})|_{\alpha\beta} \end{cases} \quad (20)$$

184 Introducing a standard variational argument to Eq. (18),  $\delta\Pi = 0$ , and  
 185 considering the arbitrariness of virtual variables,  $\delta\mathbf{v}$ ,  $\delta\varepsilon_{\alpha\beta}$ ,  $\delta\kappa_{\alpha\beta}$ ,  $N^{\alpha\beta}$ ,  $M^{\alpha\beta}$   
 186 lead to the following weak form:

$$-\int_{\Omega} h\delta\varepsilon_{\alpha\beta}C^{\alpha\beta\gamma\eta}\varepsilon_{\gamma\eta}d\Omega + \int_{\Omega} \delta\varepsilon_{\alpha\beta}N^{\alpha\beta}d\Omega = 0 \quad (21a)$$

$$-\int_{\Omega} \frac{h^3}{12}\delta\kappa_{\alpha\beta}C^{\alpha\beta\gamma\eta}\kappa_{\gamma\eta}d\Omega + \int_{\Omega} \delta\kappa_{\alpha\beta}M^{\alpha\beta}d\Omega = 0 \quad (21b)$$

$$\begin{aligned} \int_{\Omega} \delta N^{\alpha\beta}\varepsilon_{\alpha\beta}d\Omega - \int_{\Gamma} \delta\mathbf{T}_N \cdot \mathbf{v}d\Gamma + \int_{\Omega} \delta\mathbf{b}_N \cdot \mathbf{v}d\Omega \\ + \int_{\Gamma_v} \delta\mathbf{T}_N \cdot \mathbf{v}d\Gamma = \int_{\Gamma_v} \delta\mathbf{T}_N \cdot \bar{\mathbf{v}}d\Gamma \end{aligned} \quad (21c)$$

$$\begin{aligned} \int_{\Omega} \delta M^{\alpha\beta}\kappa_{\alpha\beta}d\Omega - \int_{\Gamma} \delta M_{nn}\theta_n d\Gamma + \int_{\Gamma} \delta\mathbf{T}_M \cdot \mathbf{v}d\Gamma + (\delta P\mathbf{a}_3 \cdot \mathbf{v})_{\mathbf{x} \in C} + \int_{\Omega} \delta\mathbf{b}_M \cdot \mathbf{v}d\Omega \\ + \int_{\Gamma_\theta} \delta M_{nn}\theta_n d\Gamma - \int_{\Gamma_v} \delta\mathbf{T}_M \cdot \mathbf{v}d\Gamma - (\delta P\mathbf{a}_3 \cdot \mathbf{v})_{\mathbf{x} \in C_v} \\ = \int_{\Gamma_\theta} \delta M_{nn}\bar{\theta}_n d\Gamma - \int_{\Gamma_v} \delta\mathbf{T}_M \cdot \bar{\mathbf{v}}d\Gamma - (\delta P\mathbf{a}_3 \cdot \bar{\mathbf{v}})_{\mathbf{x} \in C_v} \end{aligned} \quad (21d)$$

$$\begin{aligned} \int_{\Gamma} \delta\theta_n M_{nn}d\Gamma - \int_{\Gamma} \delta\mathbf{v} \cdot \mathbf{T}d\Gamma - (\delta\mathbf{v} \cdot \mathbf{a}_3 P)_{\mathbf{x} \in C} + \int_{\Omega} \delta\mathbf{v} \cdot \mathbf{b}d\Omega \\ - \int_{\Gamma_\theta} \delta\theta_n M_{nn}d\Gamma + \int_{\Gamma_v} \delta\mathbf{v} \cdot \mathbf{T}d\Gamma + (\delta\mathbf{v} \cdot \mathbf{a}_3 P)_{\mathbf{x} \in C_v} = - \int_{\Gamma_T} \delta\mathbf{v} \cdot \bar{\mathbf{t}}d\Gamma - \int_{\Omega} \delta\mathbf{v} \cdot \bar{\mathbf{b}}d\Omega \end{aligned} \quad (21e)$$

191 where the geometric relationships of Eq. (19) is used herein.

192    **3. Mixed meshfree formulation for modified Hellinger-Reissner-Hu-Washizu's  
193    weak form**

194    *3.1. Reproducing kernel approximation for displacement*

195    This study approximates the displacement by adopting reproducing kernel  
196    approximation. As shown in Fig. 2, the mid-surface of the shell  $\Omega$  is discretized  
197    by a set of meshfree nodes  $\{\xi_I\}_{I=1}^{n_p}$  in parametric configuration, where  $n_p$  is the  
198    total number of meshfree nodes. The approximated displacement namely  $\mathbf{v}^h$   
199    can be expressed as:

$$\mathbf{v}(\xi) = \sum_{I=1}^{n_p} \Psi_I(\xi) \mathbf{d}_I \quad (22)$$

200    in which  $\Psi_I$  and  $\mathbf{d}_I$  is represent the shape function and nodal coefficient tensor  
201    related by node  $\xi_I$ . According to reproducing kernel approximation [4], the  
202    shape function takes the following form:

$$\Psi_I(\xi) = \mathbf{p}^T(\xi) \mathbf{c}(\xi) \phi(\xi_I - \xi) \quad (23)$$

203    where  $\mathbf{p}$  is the basis function vector represented using the following quadratic  
204    function as:

$$\mathbf{p} = \{1, \xi^1, \xi^2, (\xi^1)^2, \xi^1 \xi^2, (\xi^2)^2\}^T \quad (24)$$

205    The kernel function denoted by  $\phi$  controls the support and smoothness of  
206    meshfree shape functions. The quintic B-spline function with square support is  
207    used herein as the kernel function:

$$\phi(\xi_I - \xi) = \phi(\hat{s}_1)\phi(\hat{s}_2), \quad \hat{s}_\alpha = \frac{|\xi_I^\alpha - \xi^\alpha|}{s_{\alpha I}} \quad (25)$$

208    with

$$\phi(\hat{s}_\alpha) = \frac{1}{5!} \begin{cases} (3 - 3\hat{s}_\alpha)^5 - 6(2 - 3\hat{s}_\alpha)^5 + 15(1 - 3\hat{s}_\alpha)^5 & \hat{s}_\alpha \leq \frac{1}{3} \\ (3 - 3\hat{s}_\alpha)^5 - 6(2 - 3\hat{s}_\alpha)^5 & \frac{1}{3} < \hat{s}_\alpha \leq \frac{2}{3} \\ (3 - 3\hat{s}_\alpha)^5 & \frac{2}{3} < \hat{s}_\alpha \leq 1 \\ 0 & \hat{s}_\alpha > 1 \end{cases} \quad (26)$$

209    and  $\hat{s}_{\alpha I}$  means the characterized size of support for  $s_{\alpha I}$  means the support size  
210    of meshfree shape function  $\Psi_I$ .

211    The unknown vector  $\mathbf{c}$  in shape function are determined by the fulfillment  
212    of the so-called consistency condition:

$$\sum_{I=1}^{n_p} \Psi_I(\xi) \mathbf{p}(\xi_I) = \mathbf{p}(\xi) \quad (27)$$

213    or equivalently

$$\sum_{I=1}^{n_p} \Psi_I(\xi) \mathbf{p}(\xi_I - \xi) = \mathbf{p}(\mathbf{0}) \quad (28)$$

<sup>214</sup> Substituting Eq. (22) into (28), yields:

$$\mathbf{A}(\boldsymbol{\xi})\mathbf{c}(\boldsymbol{\xi}) = \mathbf{p}(\mathbf{0}) \Rightarrow \mathbf{c}(\boldsymbol{\xi}) = \mathbf{A}^{-1}(\boldsymbol{\xi})\mathbf{p}(\mathbf{0}) \quad (29)$$

<sup>215</sup> where  $\mathbf{A}$  is the moment matrix:

$$\mathbf{A}(\boldsymbol{\xi}) = \sum_{I=1}^{n_p} \phi(\boldsymbol{\xi}_I - \boldsymbol{\xi}) \mathbf{p}(\boldsymbol{\xi}_I - \boldsymbol{\xi}) \mathbf{p}^T(\boldsymbol{\xi}_I - \boldsymbol{\xi}) \quad (30)$$

<sup>216</sup> Substituting Eq. (29) back into Eq. (22), the expression of meshfree shape  
<sup>217</sup> function can be written as:

$$\Psi_I(\boldsymbol{\xi}) = \mathbf{p}^T(\boldsymbol{\xi}_I - \boldsymbol{\xi}) \mathbf{A}^{-1}(\boldsymbol{\xi}) \mathbf{p}(\mathbf{0}) \phi(\boldsymbol{\xi}_I - \boldsymbol{\xi}) \quad (31)$$

<sup>218</sup> *3.2. Reproducing kernel gradient smoothing approximation for effective stress  
<sup>219</sup> and strain*

<sup>220</sup> In Galerkin meshfree formulation, the mid-plane of thin shell  $\Omega$  is split by  
<sup>221</sup> a set of integration cells  $\Omega_C$ 's,  $\cup_{C=1}^{n_e} \Omega_C \approx \Omega$ , as shown in Fig. 2. With the  
<sup>222</sup> inspiration of reproducing kernel smoothing framework, the Cartesian and co-  
<sup>223</sup> variant derivatives of displacement,  $\mathbf{v}_{,\alpha}$  and  $-\mathbf{v}_{,\alpha}|_\beta$ , in strains  $\varepsilon_{\alpha\beta}$ ,  $\kappa_{\alpha\beta}$  are  
<sup>224</sup> approximated by  $(p-1)$ -th order polynomials in each integration cells. In inte-  
<sup>225</sup> gration cell  $\Omega_C$ , the approximated derivatives and strains denoted by  $\mathbf{v}_{,\alpha}^h$ ,  $\varepsilon_{\alpha\beta}^h$   
<sup>226</sup> and  $-\mathbf{v}_{,\alpha}|_\beta$ ,  $\kappa_{\alpha\beta}^h$  can be expressed by:

$$\mathbf{v}_{,\alpha}^h(\boldsymbol{\xi}) = \mathbf{q}^T(\boldsymbol{\xi}) \mathbf{d}_\alpha^\varepsilon, \quad \varepsilon_{\alpha\beta}^h(\boldsymbol{\xi}) = \mathbf{q}^T(\boldsymbol{\xi}) \frac{1}{2} (\mathbf{a}_\alpha \cdot \mathbf{d}_\beta^\varepsilon + \mathbf{a}_\beta \cdot \mathbf{d}_\alpha^\varepsilon) \quad (32)$$

$$-\mathbf{v}_{,\alpha}|_\beta(\boldsymbol{\xi}) = \mathbf{q}^T(\boldsymbol{\xi}) \mathbf{d}_{\alpha\beta}^\kappa, \quad \kappa_{\alpha\beta}^h(\boldsymbol{\xi}) = \mathbf{q}^T(\boldsymbol{\xi}) \mathbf{a}_3 \cdot \mathbf{d}_{\alpha\beta}^\kappa \quad (33)$$

<sup>227</sup> where  $\mathbf{q}$  is the linear polynomial vector and has the following form:

$$\mathbf{q} = \{1, \xi^1, \xi^2\}^T \quad (34)$$

<sup>228</sup> and the  $\mathbf{d}_\alpha^\varepsilon$ ,  $\mathbf{d}_{\alpha\beta}^\kappa$  are the corresponding coefficient vector tensors. For the con-  
<sup>229</sup> ciseness, the mixed usage of tensor and vector is introduced in this study. For  
<sup>230</sup> instance, the component of coefficient tensor vector  $\mathbf{d}_{\alpha I}^\varepsilon$ ,  $\mathbf{d}_\alpha^\varepsilon = \{\mathbf{d}_{\alpha I}^\varepsilon\}$ , is a three  
<sup>231</sup> dimensional tensor,  $\dim \mathbf{d}_{\alpha I}^\varepsilon = \dim \mathbf{v}$ .

<sup>232</sup> In order to meet the integration constraint of thin shell problem, the ap-  
<sup>233</sup> proximated stresses  $N^{\alpha\beta h}$ ,  $M^{\alpha\beta h}$  are assumed to be a similar form with strains,  
<sup>234</sup> yields:

$$N^{\alpha\beta h}(\boldsymbol{\xi}) = \mathbf{q}^T(\boldsymbol{\xi}) \mathbf{a}^\alpha \cdot \mathbf{d}_N^\beta, \quad \mathbf{a}_\alpha N^{\alpha\beta h}(\boldsymbol{\xi}) = \mathbf{q}^T(\boldsymbol{\xi}) \mathbf{d}_N^\beta \quad (35)$$

$$M^{\alpha\beta h}(\boldsymbol{\xi}) = \mathbf{q}^T(\boldsymbol{\xi}) \mathbf{a}_3 \cdot \mathbf{d}_M^{\alpha\beta}, \quad \mathbf{a}_3 M^{\alpha\beta h}(\boldsymbol{\xi}) = \mathbf{q}^T(\boldsymbol{\xi}) \mathbf{d}_M^{\alpha\beta} \quad (36)$$

<sup>235</sup> substituting the approximations of Eqs. (22), (32), (33), (35), (36) into Eqs.  
<sup>236</sup> (21c), (21d) can express  $\mathbf{d}_\beta^\varepsilon$  and  $\mathbf{d}_{\alpha\beta}^\kappa$  by  $\mathbf{d}$  as:

$$\mathbf{d}_\beta^\varepsilon = \mathbf{G}^{-1} \left( \sum_{I=1}^{n_p} (\tilde{\mathbf{g}}_{\beta I} - \bar{\mathbf{g}}_{\beta I}) \mathbf{d}_I + \hat{\mathbf{g}}_\beta \right) \quad (37)$$

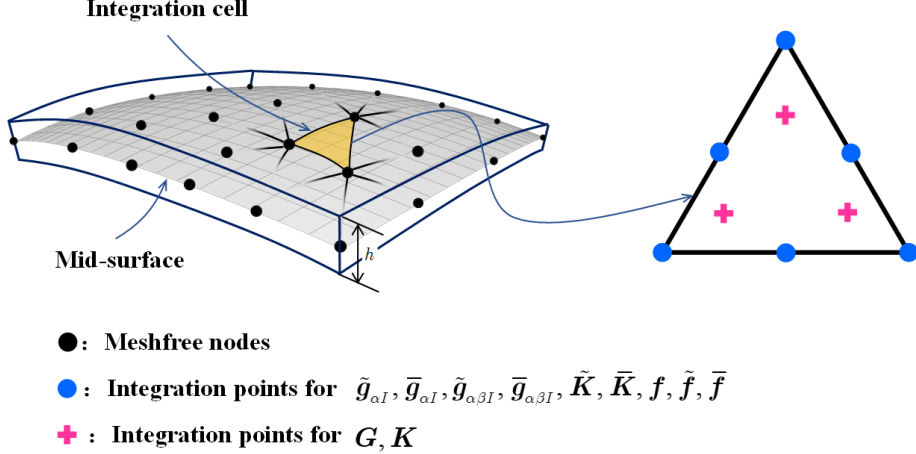


Figure 2: Integration scheme for Hu-Washizu weak form.

239

$$\mathbf{d}_{\alpha\beta}^\kappa = \mathbf{G}^{-1} \left( \sum_{I=1}^{n_p} (\tilde{\mathbf{g}}_{\alpha\beta I} - \bar{\mathbf{g}}_{\alpha\beta I}) \mathbf{d}_I + \hat{\mathbf{g}}_{\alpha\beta} \right) \quad (38)$$

240 with

$$\mathbf{G} = \int_{\Omega_C} \mathbf{q}^T \mathbf{q} d\Omega \quad (39)$$

241

$$\tilde{\mathbf{g}}_{\beta I} = \int_{\Gamma_C} \Psi_I \mathbf{q} n_\beta d\Gamma - \int_{\Omega_C} \Psi_I \mathbf{q}_{|\beta} d\Omega \quad (40a)$$

$$\bar{\mathbf{g}}_{\beta I} = \int_{\Gamma_C \cap \Gamma_v} \Psi_I \mathbf{q} n_\beta d\Gamma \quad (40b)$$

$$\hat{\mathbf{g}}_\beta = \int_{\Gamma_C \cap \Gamma_v} \mathbf{q} n_\beta \bar{\mathbf{v}} d\Gamma \quad (40c)$$

242

$$\begin{aligned} \tilde{\mathbf{g}}_{\alpha\beta I} &= \int_{\Gamma_C} \Psi_{I,\gamma} n^\gamma \mathbf{q} n_\alpha n_\beta d\Gamma - \int_{\Gamma_C} \Psi_I (\mathbf{q}_{|\beta} n_\alpha + (\mathbf{q} s_\alpha n_\beta)_{,\gamma} s^\gamma) d\Gamma \\ &\quad + [[\Psi_I \mathbf{q} s_\alpha n_\beta]]_{\mathbf{x} \in C_C} - \int_{\Omega_C} \Psi_I \mathbf{q}_{,\alpha|\beta} d\Omega \end{aligned} \quad (41a)$$

$$\begin{aligned} \bar{\mathbf{g}}_{\alpha\beta I} &= \int_{\Gamma_C \cap \Gamma_\theta} \Psi_{I,\gamma} n^\gamma \mathbf{q} n_\alpha n_\beta d\Gamma - \int_{\Gamma_C \cap \Gamma_v} \Psi_I (\mathbf{q}_{|\beta} n_\alpha + (\mathbf{q} s_\alpha n_\beta)_{,\gamma} s^\gamma) d\Gamma \\ &\quad + [[\Psi_I \mathbf{q} s_\alpha n_\beta]]_{\mathbf{x} \in C_C \cap C_v} \end{aligned} \quad (41b)$$

$$\begin{aligned} \hat{\mathbf{g}}_{\alpha\beta} &= \int_{\Gamma_C \cap \Gamma_\theta} \mathbf{q} n_\alpha n_\beta \bar{\mathbf{a}}_3 \bar{\mathbf{n}} d\Gamma - \int_{\Gamma_C \cap \Gamma_v} (\mathbf{q}_{|\beta} n_\alpha + (\mathbf{q} s_\alpha n_\beta)_{,\gamma} s^\gamma) \bar{\mathbf{v}} d\Gamma \\ &\quad + [[\mathbf{q} s_\alpha n_\beta \bar{\mathbf{v}}]]_{\mathbf{x} \in C_C \cap C_v} \end{aligned} \quad (41c)$$

<sup>243</sup> where evaluations of  $\mathbf{q}_{|\beta}$ ,  $\mathbf{q}_{\alpha|\beta}$  are detail in Appendix A. Further plugging Eqs.  
<sup>244</sup> (37) and (38) back into Eqs. (32) and (33) respectively gives the final expression  
<sup>245</sup> of  $\mathbf{v}_{,\alpha}^h$ ,  $\varepsilon_{\alpha\beta}^h$  and  $\mathbf{-v}_{,\alpha\beta}^h$ ,  $\kappa_{\alpha\beta}^h$  as:

$$\mathbf{v}_{,\alpha}^h = \sum_{I=1}^{n_p} (\tilde{\Psi}_{I,\alpha} - \bar{\Psi}_{I,\alpha}) \mathbf{d}_I + \mathbf{q}^T \mathbf{G}^{-1} \hat{\mathbf{g}}_\alpha \quad (42a)$$

$$\begin{aligned} \varepsilon_{\alpha\beta}^h &= \sum_{I=1}^{n_p} \frac{1}{2} (\mathbf{a}_\alpha \tilde{\Psi}_{I,\beta} + \mathbf{a}_\beta \tilde{\Psi}_{I,\alpha}) \cdot \mathbf{d}_I - \sum_{I=1}^{n_p} \frac{1}{2} (\mathbf{a}_\alpha \bar{\Psi}_{I,\beta} + \mathbf{a}_\beta \bar{\Psi}_{I,\alpha}) \cdot \mathbf{d}_I \\ &\quad + \mathbf{q}^T \mathbf{G}^{-1} \frac{1}{2} (\mathbf{a}_\alpha \cdot \hat{\mathbf{g}}_\beta + \mathbf{a}_\beta \cdot \hat{\mathbf{g}}_\alpha) \\ &= \tilde{\varepsilon}_{\alpha\beta}^h - \bar{\varepsilon}_{\alpha\beta}^h + \hat{\varepsilon}_{\alpha\beta}^h \end{aligned} \quad (42b)$$

$$-\mathbf{v}_{,\alpha}^h|_\beta = \sum_{I=1}^{n_p} (\tilde{\Psi}_{I,\alpha\beta} - \bar{\Psi}_{I,\alpha\beta}) \mathbf{d}_I + \mathbf{q}^T \mathbf{G}^{-1} \hat{\mathbf{g}}_{\alpha\beta} \quad (43a)$$

$$\begin{aligned} \kappa_{\alpha\beta}^h &= \sum_{I=1}^{n_p} \tilde{\Psi}_{I,\alpha\beta} \mathbf{a}_3 \cdot \mathbf{d}_I - \sum_{I=1}^{n_p} \bar{\Psi}_{I,\alpha\beta} \mathbf{a}_3 \cdot \mathbf{d}_I + \mathbf{q}^T \mathbf{G}^{-1} \mathbf{a}_3 \cdot \hat{\mathbf{g}}_{\alpha\beta} \\ &= \tilde{\kappa}_{\alpha\beta}^h - \bar{\kappa}_{\alpha\beta}^h + \hat{\kappa}_{\alpha\beta}^h \end{aligned} \quad (43b)$$

<sup>249</sup> with

$$\begin{cases} \tilde{\varepsilon}_{\alpha\beta}^h = \sum_{I=1}^{n_p} \frac{1}{2} (\mathbf{a}_\alpha \tilde{\Psi}_{I,\beta} + \mathbf{a}_\beta \tilde{\Psi}_{I,\alpha}) \cdot \mathbf{d}_I = \sum_{I=1}^{n_p} \tilde{\varepsilon}_{\alpha\beta I} \cdot \mathbf{d}_I \\ \bar{\varepsilon}_{\alpha\beta}^h = \sum_{I=1}^{n_p} \frac{1}{2} (\mathbf{a}_\alpha \bar{\Psi}_{I,\beta} + \mathbf{a}_\beta \bar{\Psi}_{I,\alpha}) \cdot \mathbf{d}_I = \sum_{I=1}^{n_p} \bar{\varepsilon}_{\alpha\beta I} \cdot \mathbf{d}_I \\ \hat{\varepsilon}_{\alpha\beta}^h = \mathbf{q}^T \mathbf{G}^{-1} \frac{1}{2} (\mathbf{a}_\alpha \cdot \hat{\mathbf{g}}_\beta + \mathbf{a}_\beta \cdot \hat{\mathbf{g}}_\alpha) \end{cases} \quad (44)$$

$$\begin{cases} \tilde{\Psi}_{I,\alpha}(\boldsymbol{\xi}) = \mathbf{q}^T(\boldsymbol{\xi}) \mathbf{G}^{-1} \tilde{\mathbf{g}}_{\alpha I} \\ \bar{\Psi}_{I,\alpha}(\boldsymbol{\xi}) = \mathbf{q}^T(\boldsymbol{\xi}) \mathbf{G}^{-1} \bar{\mathbf{g}}_{\alpha I} \\ \tilde{\varepsilon}_{\alpha\beta I} = \frac{1}{2} (\mathbf{a}_\alpha \tilde{\Psi}_{I,\beta} + \mathbf{a}_\beta \tilde{\Psi}_{I,\alpha}) \\ \bar{\varepsilon}_{\alpha\beta I} = \frac{1}{2} (\mathbf{a}_\alpha \bar{\Psi}_{I,\beta} + \mathbf{a}_\beta \bar{\Psi}_{I,\alpha}) \end{cases} \quad (45)$$

$$\begin{cases} \tilde{\kappa}_{\alpha\beta}^h = \sum_{I=1}^{n_p} \tilde{\Psi}_{I,\alpha\beta} \mathbf{a}_3 \cdot \mathbf{d}_I = \sum_{I=1}^{n_p} \tilde{\kappa}_{\alpha\beta I} \cdot \mathbf{d}_I \\ \bar{\kappa}_{\alpha\beta}^h = \sum_{I=1}^{n_p} \bar{\Psi}_{I,\alpha\beta} \mathbf{a}_3 \cdot \mathbf{d}_I = \sum_{I=1}^{n_p} \bar{\kappa}_{\alpha\beta I} \cdot \mathbf{d}_I \\ \hat{\kappa}_{\alpha\beta}^h = \mathbf{q}^T \mathbf{G}^{-1} \mathbf{a}_3 \cdot \hat{\mathbf{g}}_{\alpha\beta} \end{cases} \quad (46)$$

252

$$\begin{cases} \tilde{\Psi}_{I,\alpha\beta}(\xi) = \mathbf{q}^T(\xi) \mathbf{G}^{-1} \tilde{\mathbf{g}}_{\alpha\beta I} \\ \bar{\Psi}_{I,\alpha\beta}(\xi) = \mathbf{q}^T(\xi) \mathbf{G}^{-1} \tilde{\mathbf{g}}_{\alpha\beta I} \\ \tilde{\kappa}_{\alpha\beta I} = \tilde{\Psi}_{I,\alpha\beta} \mathbf{a}_3 \\ \bar{\kappa}_{\alpha\beta I} = \bar{\Psi}_{I,\alpha\beta} \mathbf{a}_3 \end{cases} \quad (47)$$

253 It has to be noted that, referring to reproducing kernel gradient smoothing  
 254 framework [26],  $\tilde{\Psi}_{I,\alpha}$ ,  $\tilde{\Psi}_{I,\alpha\beta}$  are actually the first and second order smoothed  
 255 gradients in curvilinear coordinates.  $\tilde{\mathbf{g}}_{\alpha I}$  and  $\tilde{\mathbf{g}}_{\alpha\beta I}$  are the right hand side inte-  
 256 gration constraints for first and second order gradients, then this formulation can  
 257 meet the variational consistency for the  ~~$p$ -th second~~ order polynomials. It should  
 258 be known that, in curved model, the variational consistency for non-polynomial  
 259 functions, like trigonometric functions, should be required for the polynomial  
 260 solution. Even with  ~~$p$ -th order high order polynomial~~ variational consistency,  
 261 the proposed formulation can not exactly reproduce the solution spanned by  
 262 basis functions. However, the accuracy of reproducing kernel smoothed gradi-  
 263 ents is still better than traditional meshfree formulation. Numerical examples  
 264 in the section below will provide better evidence to prove the accuracy of the  
 265 reproducing kernel smoothed gradients.

<sup>266</sup> 4. Naturally variational enforcement for essential boundary condi-  
<sup>267</sup> tions

<sup>268</sup> 4.1. Discrete equilibrium equations

<sup>269</sup> With the approximated effective stresses and strains, the last equation of  
<sup>270</sup> weak form Eq. (21e) becomes:

$$-\sum_{C=1}^{n_e} \sum_{I=1}^{n_p} \delta \mathbf{d}_I \cdot \left( (\tilde{\mathbf{g}}_{\alpha I}^T - \bar{\mathbf{g}}_{\alpha I}^T) \mathbf{d}_N^\alpha + (\tilde{\mathbf{g}}_{\alpha\beta I}^T - \bar{\mathbf{g}}_{\alpha\beta I}^T) \mathbf{d}_M^{\alpha\beta} \right) = -\sum_{I=1}^{n_p} \delta \underline{\mathbf{d}}_I \cdot \mathbf{f}_I \quad (48)$$

<sup>271</sup> where  $\mathbf{f}_I$ 's are the components of the traditional force vector:

$$\mathbf{f}_I = \int_{\Gamma_t} \Psi_I \bar{\mathbf{t}} d\Gamma - \int_{\Gamma_M} \Psi_{I,\gamma} n^\gamma \bar{M}_{\mathbf{n}\mathbf{n}} d\Gamma + [[\Psi_I \mathbf{a}_3 \bar{P}]]_{\mathbf{x} \in C_P} + \int_{\Omega} \Psi_I \bar{\mathbf{b}} d\Omega \quad (49)$$

<sup>272</sup> The left side of Eq. (48) can be simplified using the following steps. For clarity,  
<sup>273</sup> the derivation of first term in Eq. (48) taken as an example is given by:

$$\begin{aligned} \sum_{I=1}^{n_p} \delta \mathbf{d}_I \cdot \tilde{\mathbf{g}}_{\alpha I}^T \mathbf{d}_N^\alpha &= \sum_{I=1}^{n_p} \delta \mathbf{d}_I \cdot (\mathbf{G}^{-1} \tilde{\mathbf{g}}_{\alpha I})^T \mathbf{G} \mathbf{d}_N^\alpha \\ &= \int_{\Omega_C} \sum_{I=1}^{n_p} \delta \mathbf{d}_I \cdot (\mathbf{q}^T \mathbf{G}^{-1} \tilde{\mathbf{g}}_{\alpha I}) \underline{\mathbf{q}}^T \mathbf{d}_N^\alpha d\Omega \\ &= \int_{\Omega_C} \sum_{I=1}^{n_p} \delta \mathbf{d}_I \cdot \mathbf{a}_\beta (\mathbf{q}^T \mathbf{G}^{-1} \tilde{\mathbf{g}}_{\alpha I}) \underline{\mathbf{q}}^T N^{\alpha\beta h} d\Omega \\ &= \int_{\Omega_C} \delta \hat{\varepsilon}_{\alpha\beta}^h N^{\alpha\beta h} d\Omega \end{aligned} \quad (50)$$

<sup>274</sup> following the above procedure and including the weak form of Eqs. (21a), (21b),  
<sup>275</sup> the left side of Eq. (48) in  $\Omega_C$  becomes:

$$\begin{aligned}
& \sum_{I=1}^{n_p} \delta \mathbf{d}_I \cdot \left( (\tilde{\mathbf{g}}_{\alpha I}^T - \bar{\mathbf{g}}_{\alpha I}^T) \mathbf{d}_N^\alpha + (\tilde{\mathbf{g}}_{\alpha \beta I}^T - \bar{\mathbf{g}}_{\alpha \beta I}^T) \mathbf{d}_M^{\alpha \beta} \right) \\
& = \int_{\Omega_C} ((\delta \tilde{\varepsilon}_{\alpha \beta}^h - \delta \bar{\varepsilon}_{\alpha \beta}^h) N^{\alpha \beta h} + (\delta \tilde{\kappa}_{\alpha \beta}^h - \delta \bar{\kappa}_{\alpha \beta}^h) M^{\alpha \beta h}) d\Omega \\
& = \int_{\Omega_C} (\delta \tilde{\varepsilon}_{\alpha \beta}^h - \delta \bar{\varepsilon}_{\alpha \beta}^h) h C^{\alpha \beta \gamma \eta} \tilde{\varepsilon}_{\gamma \eta}^h + (\delta \tilde{\kappa}_{\alpha \beta}^h - \delta \bar{\kappa}_{\alpha \beta}^h) \frac{h^3}{12} C^{\alpha \beta \gamma \eta} \tilde{\kappa}_{\gamma \eta}^h \\
& = \int_{\Omega_C} \delta \tilde{\varepsilon}_{\alpha \beta}^h h C^{\alpha \beta \gamma \eta} \tilde{\varepsilon}_{\gamma \eta}^h d\Omega + \int_{\Omega_C} \delta \tilde{\kappa}_{\alpha \beta}^h \frac{h^3}{12} C^{\alpha \beta \gamma \eta} \tilde{\kappa}_{\gamma \eta}^h d\Omega \\
& - \int_{\Omega_C} \delta \tilde{\varepsilon}_{\alpha \beta}^h h C^{\alpha \beta \gamma \eta} \bar{\varepsilon}_{\gamma \eta}^h d\Omega - \int_{\Omega_C} \delta \tilde{\varepsilon}_{\alpha \beta}^h h C^{\alpha \beta \gamma \eta} \tilde{\varepsilon}_{\gamma \eta}^h d\Omega \\
& - \int_{\Omega_C} \delta \tilde{\kappa}_{\alpha \beta}^h \frac{h^3}{12} C^{\alpha \beta \gamma \eta} \bar{\kappa}_{\gamma \eta}^h d\Omega - \int_{\Omega_C} \delta \tilde{\kappa}_{\alpha \beta}^h \frac{h^3}{12} C^{\alpha \beta \gamma \eta} \tilde{\kappa}_{\gamma \eta}^h d\Omega \\
& + \int_{\Omega_C} \delta \tilde{\varepsilon}_{\alpha \beta}^h h C^{\alpha \beta \gamma \eta} \bar{\varepsilon}_{\gamma \eta}^h d\Omega + \int_{\Omega_C} \delta \tilde{\kappa}_{\alpha \beta}^h \frac{h^3}{12} C^{\alpha \beta \gamma \eta} \bar{\kappa}_{\gamma \eta}^h d\Omega \\
& + \int_{\Omega_C} (\delta \tilde{\varepsilon}_{\alpha \beta}^h - \delta \bar{\varepsilon}_{\alpha \beta}^h) h C^{\alpha \beta \gamma \eta} \tilde{\varepsilon}_{\gamma \eta}^h d\Omega + \int_{\Omega_C} (\delta \tilde{\kappa}_{\alpha \beta}^h - \delta \bar{\kappa}_{\alpha \beta}^h) \frac{h^3}{12} C^{\alpha \beta \gamma \eta} \tilde{\kappa}_{\gamma \eta}^h d\Omega
\end{aligned} \tag{51}$$

<sup>276</sup> on further substituting Eqs. (44) and (46) into above equation gives the final  
<sup>277</sup> discrete equilibrium equations, respectively:

$$(\mathbf{K} + \tilde{\mathbf{K}} + \bar{\mathbf{K}}) \mathbf{d} = \mathbf{f} + \tilde{\mathbf{f}} + \bar{\mathbf{f}} \tag{52}$$

<sup>278</sup> where the components of stiffness matrices and force vectors in discrete equilibrium  
<sup>279</sup> equations can be evaluated as follows:

$$\mathbf{K}_{IJ} = \int_{\Omega} \tilde{\varepsilon}_{\alpha \beta I} h C^{\alpha \beta \gamma \eta} \tilde{\varepsilon}_{\gamma \eta J} d\Omega + \int_{\Omega} \tilde{\kappa}_{\alpha \beta I} \frac{h^3}{12} C^{\alpha \beta \gamma \eta} \tilde{\kappa}_{\alpha \beta \underline{\gamma} \underline{\eta} J} d\Omega \tag{53}$$

<sup>280</sup>

$$\begin{aligned}
\tilde{\mathbf{K}}_{IJ} & = - \int_{\Gamma_v} (\Psi_I \tilde{T}_{NJ} + \tilde{T}_{\underline{N} \underline{J} \underline{N} \underline{I}} \Psi_J) d\Gamma \\
& + \int_{\Gamma_\theta} (\Psi_{I,\gamma} n^\gamma \mathbf{a}_3 \tilde{\mathbf{M}}_{nnJ} + \mathbf{a}_3 \tilde{\mathbf{M}}_{nnI} \Psi_{I,\gamma \underline{J} \underline{\gamma}} n^\gamma) d\Gamma \\
& + ([[\Psi_I \mathbf{a}_3 \tilde{\mathbf{P}}_J]] + [[\tilde{\mathbf{P}}_I \mathbf{a}_3 \Psi_J]])_{x \in C_v}
\end{aligned} \tag{54a}$$

$$\tilde{\mathbf{f}}_I = - \int_{\Gamma_v} \tilde{T}_{NI} \cdot \bar{\mathbf{v}} d\Gamma + \int_{\Gamma_\theta} \tilde{\mathbf{M}}_{nnI} \bar{\theta}_n d\Gamma + [[\tilde{\mathbf{P}}_I \mathbf{a}_3 \cdot \bar{\mathbf{v}}]]_{x \in C_v} \tag{54b}$$

<sup>281</sup>

$$\bar{\mathbf{K}}_{IJ} = - \int_{\Gamma_v} \bar{T}_{MI} \Psi_J d\Gamma + \int_{\Gamma_\theta} \mathbf{a}_3 \bar{\mathbf{M}}_{nnI} \Psi_{J,\gamma} n^\gamma d\Gamma + [[\bar{\mathbf{P}}_I \mathbf{a}_3 \Psi_J]]_{x \in C_v} \tag{55a}$$

$$\bar{\mathbf{f}}_I = - \int_{\Gamma_v} \bar{T}_{MI} \cdot \bar{\mathbf{v}} d\Gamma + \int_{\Gamma_\theta} \bar{\mathbf{M}}_{nnI} \bar{\theta}_n d\Gamma + [[\bar{\mathbf{P}}_I \mathbf{a}_3 \cdot \bar{\mathbf{v}}]]_{x \in C_v} \tag{55b}$$

282 The detailed derivations of Eqs (53)-(55) are listed in the Appendix B.  
 283 As shown in these equations, Eq. (53) is the conventional stiffness matrix  
 284 evaluated by smoothed gradients  $\tilde{\Psi}_{I,\alpha}$ ,  $\tilde{\Psi}_{I,\alpha}|_{\beta}$ , and the Eqs. (54) and (55)  
 285 contribute for the enforcement of essential boundary. It should be mentioned  
 286 that, in accordance with reproducing kernel smoothed gradient framework, the  
 287 integration scheme of Eqs. (53-55) should be aligned with the those used in  
 288 the construction of smoothed gradients. The integration scheme used for pro-  
 289 posed method is shown in Fig. 2, ~~the in which the total number of the blue~~  
 290 ~~circular integration points has been optimized from a global point of view,~~  
 291 ~~aiming to reduce the computation of traditional meshfree shape functions and~~  
 292 ~~its first order derivatives. In contrast, for assembly stiffness matrix  $K$ , the~~  
 293 ~~low order Gauss integration rule is suitable to ensure the accuracy due to the~~  
 294 ~~inherently variational consistency in smoothed gradients. The detailed pos-~~  
 295 ~~tions and weight of integration points and the efficiency demonstration of this~~  
 296 ~~optimized integration scheme~~ can be found in [33]-[26, 33]. With a close look  
 297 at Eqs. (54) and (55), the proposed approach for enforcing essential boundary  
 298 conditions show an identical structure with traditional Nitsche's method, both  
 299 have the consistent and stabilized terms. So, the next subsection will review  
 300 the Nitsche's method and compare it with the proposed method.

#### 301 4.2. Comparison with Nitsche's method

302 The Nitsche's method for enforcing essential boundaries can be regarded as a  
 303 combination of Lagrangian multiplier method and penalty method, in which the  
 304 Lagrangian multiplier is represented by the approximated displacement. The  
 305 corresponding total potential energy functional  $\Pi_P$  is given by:

$$\begin{aligned}
 \Pi_P(\mathbf{v}) = & \int_{\Omega} \frac{1}{2} \varepsilon_{\alpha\beta} N^{\alpha\beta} d\Omega + \int_{\Omega} \frac{1}{2} \kappa_{\alpha\beta} M^{\alpha\beta} d\Omega \\
 & - \int_{\Gamma_t} \mathbf{v} \cdot \bar{\mathbf{t}} d\Gamma + \int_{\Gamma_M} \mathbf{v}_{,\gamma} n^{\gamma} \mathbf{a}_3 M_{\mathbf{n}\mathbf{n}} d\Gamma + (\mathbf{v} \cdot \mathbf{a}_3 P)_{\mathbf{x} \in C_P} - \int_{\Omega} \mathbf{v} \cdot \bar{\mathbf{b}} d\Omega \\
 & - \underbrace{\int_{\Gamma_v} \mathbf{t} \cdot (\mathbf{v} - \bar{\mathbf{v}}) d\Gamma + \int_{\Gamma_{\theta}} M_{\mathbf{n}\mathbf{n}} (\theta_{\mathbf{n}} - \bar{\theta}_{\mathbf{n}}) d\Gamma + (P \mathbf{a}_3 \cdot (\mathbf{v} - \bar{\mathbf{v}}))_{\mathbf{x} \in C_v}}_{\text{consistent term}} \quad (56) \\
 & + \underbrace{\sum_{i=1}^3 \frac{\alpha_{\mathbf{v}\mathbf{v}_i}}{2} \int_{\Gamma_v} (\mathbf{v} \cdot \mathbf{a}_i)^2 \mathbf{v} d\Gamma + \frac{\alpha_{\theta}}{2} \int_{\Gamma_{\theta}} \theta_{\mathbf{n}}^2 d\Gamma + \frac{\alpha_C}{2} (\mathbf{v} \cdot \mathbf{a}_3)^2 \mathbf{v} }_{\text{stabilized term}}
 \end{aligned}$$

306 where the consistent term generated from the Lagrangian multiplier method  
 307 contributes to enforce the essential boundary, and meet the variational con-  
 308 sistency condition. However, the consistent term can not always ensure the  
 309 coercivity of stiffness, so the penalty method is introduced to serve as a sta-  
 310 bilized term, ~~in which  $\alpha_{\mathbf{v}_i}$  is the experimental artificial parameter for enforcing~~  
 311 ~~the displacement towards  $\mathbf{a}_i$  direction,  $\alpha_{\theta}$  and  $\alpha_C$  are parameters for enforcing~~

<sup>312</sup> rotation and corner deflection. With a standard variational argument, the cor-  
<sup>313</sup> responding weak form can be stated as:

$$\begin{aligned}
\delta\Pi_P(\mathbf{v}) &= \int_{\Omega} \delta\varepsilon_{\alpha\beta} N^{\alpha\beta} d\Omega + \int_{\Omega} \delta\kappa_{\alpha\beta} M^{\alpha\beta} d\Omega \\
&\quad - \int_{\Gamma_t} \delta\mathbf{v} \cdot \bar{\mathbf{t}} d\Gamma + \int_{\Gamma_M} \delta\mathbf{v}_{,\gamma} n^\gamma \mathbf{a}_3 M_{\mathbf{n}\mathbf{n}} d\Gamma + (\delta\mathbf{v} \cdot \mathbf{a}_3 P)_{\mathbf{x} \in C_P} - \int_{\Omega} \delta\mathbf{v} \cdot \bar{\mathbf{b}} d\Omega \\
&\quad - \int_{\Gamma_v} \delta\mathbf{v} \cdot \mathbf{t} d\Gamma + \int_{\Gamma_\theta} \delta\theta_{\mathbf{n}} M_{\mathbf{n}\mathbf{n}} d\Gamma + (\mathbf{v} \cdot \mathbf{a}_3 P)_{\mathbf{x} \in C_v} \\
&\quad - \int_{\Gamma_v} \delta\mathbf{t} \cdot (\mathbf{v} - \bar{\mathbf{v}}) d\Gamma + \int_{\Gamma_\theta} \delta M_{\mathbf{n}\mathbf{n}} (\theta_{\mathbf{n}} - \bar{\theta}_{\mathbf{n}}) d\Gamma + (\delta P \mathbf{a}_3 \cdot (\mathbf{v} - \bar{\mathbf{v}}))_{\mathbf{x} \in C_v} \\
&\quad + \sum_{\substack{i=1 \\ \text{underlined}}}^3 \alpha_{\underline{\mathbf{v}} \underline{\mathbf{v}} \underline{i}} \int_{\Gamma_v} (\delta\mathbf{v} \cdot \underline{\mathbf{a}}_i) (\underline{\mathbf{a}}_i \cdot \mathbf{v}) d\Gamma + \alpha_\theta \int_{\Gamma_\theta} \delta\theta_{\mathbf{n}} \theta_{\mathbf{n}} d\Gamma + \alpha_C (\delta\mathbf{v} \cdot \underline{\mathbf{a}}_3 \underline{\mathbf{a}}_3 \cdot \mathbf{v})_{\mathbf{x} \in C_v} \\
&= 0
\end{aligned} \tag{57}$$

<sup>314</sup> ~~in which  $\alpha_v$ ,  $\alpha_\theta$  and  $\alpha_C$  represent experimental artificial parameters.~~ Further  
<sup>315</sup> invoking the conventional reproducing kernel approximation of Eq. (22) leads  
<sup>316</sup> to the following discrete equilibrium equations:

$$\sum_{J=1}^{n_p} (\mathbf{K}_{IJ} + \mathbf{K}^c_{IJ} + \mathbf{K}^s_{IJ}) \mathbf{d}_J = \mathbf{f}_I + \mathbf{f}^c + \mathbf{f}^s \tag{58}$$

<sup>317</sup> where the stiffness  $\mathbf{K}_{IJ}$  is identical with Eq. (53).  ~~$\mathbf{K}_{IJ}^c$  and  $\mathbf{K}_{IJ}^s$~~   $\mathbf{K}^c$  and  
<sup>318</sup>  $\mathbf{K}^s$  are the stiffness matrices for consistent and stabilized terms, respectively,  
<sup>319</sup> and their components have the following form:

$$\begin{aligned}
\mathbf{K}_{IJ}^c &= - \int_{\Gamma_v} (\Psi_I \mathbf{T}_{NJ} + \mathbf{T}_{\underline{N}J \underline{N}I} \Psi_J) d\Gamma \\
&\quad + \int_{\Gamma_\theta} (\Psi_{I,\gamma} n^\gamma \mathbf{a}_3 M_{\mathbf{n}\mathbf{n}J} + \mathbf{a}_3 M_{\mathbf{n}\mathbf{n}I} \Psi_{I,\gamma \underline{J} \underline{\gamma}} n^\gamma) d\Gamma \\
&\quad + ([[ \Psi_I \mathbf{a}_3 \mathbf{P}_J ]]] + [[ \mathbf{P}_I \mathbf{a}_3 \Psi_J ]])_{\mathbf{x} \in C_v}
\end{aligned} \tag{59a}$$

$$\mathbf{f}_I^c = - \int_{\Gamma_v} \mathbf{T}_I \cdot \bar{\mathbf{v}} d\Gamma + \int_{\Gamma_\theta} \mathbf{M}_{\mathbf{n}\mathbf{n}I} \bar{\theta}_{\mathbf{n}} d\Gamma + [[ \mathbf{P}_I \mathbf{a}_3 \cdot \bar{\mathbf{v}} ]]_{\mathbf{x} \in C_v} \tag{59b}$$

<sup>320</sup>

$$\mathbf{K}_{IJ}^s = \underline{\alpha_v} \underline{\alpha_v} \int_{\Gamma_v} \Psi_I \Psi_J \mathbf{1} d\Gamma + \alpha_\theta \int_{\Gamma_\theta} \Psi_{I,\eta} n^\eta \mathbf{a}_3 \mathbf{a}_3 n^\gamma \Psi_{J,\gamma} d\Gamma + \alpha_C [[ \Psi_I \mathbf{a}_3 \mathbf{a}_3 \Psi_J ]]_{\mathbf{x} \in C_v} \tag{60a}$$

$$\mathbf{f}_I^s = \underline{\alpha_v} \underline{\alpha_v} \int_{\Gamma_v} \Psi_I \bar{\mathbf{v}} d\Gamma + \alpha_\theta \int_{\Gamma_\theta} \Psi_{I,\eta} n^\eta \mathbf{a}_3 \bar{\theta}_{\mathbf{n}} d\Gamma + \alpha_C [[ \Psi_I \mathbf{a}_3 \mathbf{a}_3 \cdot \bar{\mathbf{v}} ]]_{\mathbf{x} \in C_v} \tag{60b}$$

<sup>321</sup> with

$$\alpha_v = \begin{bmatrix} \alpha_{v1} & 0 & 0 \\ 0 & \alpha_{v2} & 0 \\ 0 & 0 & \alpha_{v3} \end{bmatrix} \quad (61)$$

<sup>322</sup> On comparing with the consistent terms of Eqs. (54) and (59), the expres-  
<sup>323</sup> sions were almost identical, the major difference is that the higher order deriva-  
<sup>324</sup> tives of shape functions have been replaced by smoothed gradients. Owing to  
<sup>325</sup> the reproducing kernel framework, the construction of smoothed gradients only  
<sup>326</sup> concerned about the computation of traditional meshfree shape functions and  
<sup>327</sup> their first order derivatives, which avoid the costly computation of higher or-  
<sup>328</sup> der derivatives. Moreover, the stabilized terms in Eq. (60) employs the penalty  
<sup>329</sup> method with big enough artificial parameters to ensure the coercivity of stiffness.  
<sup>330</sup> And the optimal values of these artificial parameters are proportional to the  
<sup>331</sup> grid size of discrete model that can be represented by support size in meshfree  
<sup>332</sup> approximation, where the  $\alpha_{v\alpha} \propto s^{-1}$ ,  $\alpha_{v3} \propto s^{-3}$ ,  $\alpha_\theta \propto s^{-1}$ ,  $\alpha_C \propto s^{-2}$ [31], and  
<sup>333</sup>  $s = \min\{s_{all}\}$ . In contrast, the stabilized term of Eq. (55) naturally exists in  
<sup>334</sup> its weak form, and can stabilize the result without considering any artificial  
<sup>335</sup> parameters.

336    **5. Numerical examples**

337    The suggested method, which uses Nitsche's method, the consistent repro-  
 338    ducing kernel gradient smoothing integration scheme (RKGSI), and the non-  
 339    consistent Gauss integration scheme (GI) with penalty method, as well as the  
 340    proposed Hu-Washizu formulation (HW) to enforce the necessary boundary con-  
 341    ditions, is validated in this section through several examples. A normalized  
 342    support size of 2.5 is used for all the methods to ensure the requirement of  
 343    quadratic base meshfree approximation. To eliminate the influence of integra-  
 344    tion, the Gauss integration scheme uses 6 Gauss points for domain integration  
 345    and 3 points for boundary integration, so as to maintain the same integration  
 346    accuracy between domain and boundaries. Moreover, the number of integra-  
 347    tion points are identical between the Gauss and RKGSI schemes. The error  
 348    estimates of displacement ( $L_2$ -Error) and energy ( $H_e$ -Error) is used here:

$$L_2\text{-Error} = \frac{\sqrt{\int_{\Omega}(\mathbf{v} - \mathbf{v}^h) \cdot (\mathbf{v} - \mathbf{v}^h) d\Omega}}{\sqrt{\mathbf{v} \cdot \mathbf{v}}}$$

$$H_e\text{-Error} = \frac{\sqrt{\int_{\Omega} \left( (\varepsilon_{\alpha\beta} - \varepsilon_{\alpha\beta}^h)(N^{\alpha\beta} - N^{\alpha\beta h}) + \int_{\Omega} (\kappa_{\alpha\beta} - \kappa_{\alpha\beta}^h)(M^{\alpha\beta} - M^{\alpha\beta h}) \right) d\Omega}}{\sqrt{\int_{\Omega} (\varepsilon_{\alpha\beta} N^{\alpha\beta} + \kappa_{\alpha\beta} M^{\alpha\beta}) d\Omega}}$$
(62)

349    **5.1. Patch tests**

350    The linear and quadratic patch tests for flat and curved thin shells are  
 351    firstly studied to verify the variational consistency of the proposed method.  
 352    As shown in Fig. 3, the flat and curved models are depicted by an identical  
 353    parametric domain  $\Omega = (0, 1) \otimes (0, 1)$ , where the cylindrical coordinate sys-  
 354    tem with radius  $R = 1$ , thickness  $h = 0.1$  is employed to describe the curved  
 355    model, and the whole domain  $\Omega$  is discretized by the 165 meshfree nodes. The  
 356    Young's modulus and Poisson's ratio of thin shell are set to  $E = 1$ ,  $\nu = 0$ .  
 357    The artificial parameters of  $\alpha_v = 10^5 \times E$ ,  $\alpha_\theta = 10^3 \times E$ ,  $\alpha_C = 10^5 \times E$  and  
 358     $\alpha_v = 10^9 \times E$ ,  $\alpha_\theta = 10^9 \times E$ ,  $\alpha_C = 10^9 \times E$  are used for Nitsche's method and  
 359    penalty method respectively.

360    All the boundaries are enforced as essential boundary conditions with the following manufactured exact solution:

$$\mathbf{v} = \begin{cases} (\xi^1 + 2\xi^2)^n \\ (3\xi^1 + 4\xi^2)^n \\ (5\xi^1 + 6\xi^2)^n \end{cases}, \quad n = \begin{cases} 1 & \text{Linear patch test} \\ 2 & \text{Quadratic patch test} \end{cases}$$
(63)

361    Table 1 lists the  $L_2$ - and  $H_e$ -Error results of patch test with flat model, where  
 362    the RKGSI scheme with variational consistent essential boundary enforcement,  
 363    i.e. RKGSI-Nitsche and RKGSI-HW, can pass the linear and quadratic patch  
 364    test. In contrast, the RKGSI-Penalty cannot pass the patch test since the  
 365    Penalty method is unable to ensure the variational consistency. Due to the  
 366    loss of variational consistency condition, even with Nitsche's method, Gauss

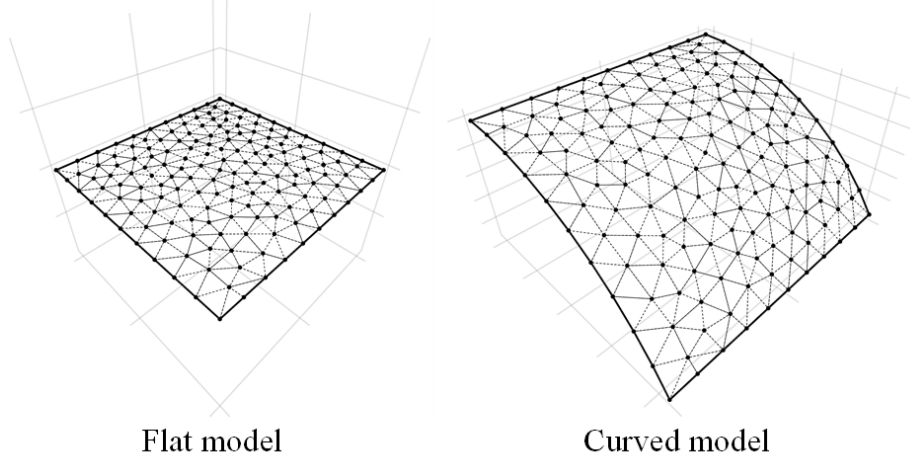


Figure 3: Meshfree discretization for patch test

meshfree formulations show noticeable errors. Table 2 shows the results for curved model, which indicated that all the considered methods cannot pass the patch test. This is mainly because the proposed smoothed gradient of Eqs. (35) and (36) could not exactly reproduce the non-polynomial membrane and bending stress. However, the RKGSI-HW and RKGSI-Nitsche methods also provide better accuracy compared to others due to the fulfillment of first second-order variational consistency. And, even only with local variational consistency, the RKGSI-Penalty obtained a better result than traditional Gauss scheme. Meanwhile, the bending moment contours of  $M^{12}$  are listed in Fig. 4, which further verify that the proposed method provided a satisfactory result compared to exact solution. On the other hand, the RKGSI-Penalty and the conventional Gauss meshfree formulations showed errors.

Table 1: Results of patch test for flat model.

	Linear patch test		Quadratic patch test	
	$L_2$ -Error	$H_e$ -Error	$L_2$ -Error	$H_e$ -Error
GI-Penalty	$4.45E-4$	$4.45E-04$	$1.35E-2$	$1.35E-02$
GI-Nitsche	$4.51E-4$	$4.51E-04$	$1.42E-2$	$1.42E-02$
RKGSI-Penalty	$3.64E-9$	$3.64E-09$	$6.77E-8$	$6.77E-08$
RKGSI-Nitsche	$3.31E-12$	$3.31E-12$	$1.34E-11$	$1.34E-11$
RKGSI-HR	$6.67E-13$	$6.67E-13$	$1.50E-11$	$1.50E-11$

### 5.2. Scordelis-Lo roof

This example considers the classical Scordelis-Lo roof problem, as depicted in Fig. 5. The cylindrical roof has dimensions  $R = 25$ ,  $L = 50$ ,  $h = 0.25$ ,

Table 2: Results of patch test for cylindrical model.

	Linear patch test		Quadratic patch test	
	$L_2$ -Error	$H_e$ -Error	$L_2$ -Error	$H_e$ -Error
GI-Penalty	$3.79E-4$	$3.79E-04$	$1.30E-2$	$1.30E-02$
GI-Nitsche	$4.04E-4$	$4.04E-04$	$1.42E-2$	$1.42E-02$
RKGSI-Penalty	$1.47E-4$	$1.47E-04$	$5.39E-3$	$5.39E-03$
RKGSI-Nitsche	$2.41E-6$	$2.41E-06$	$7.37E-5$	$7.37E-05$
RKGSI-HR	$4.28E-6$	$4.28E-06$	$1.30E-4$	$1.30E-04$

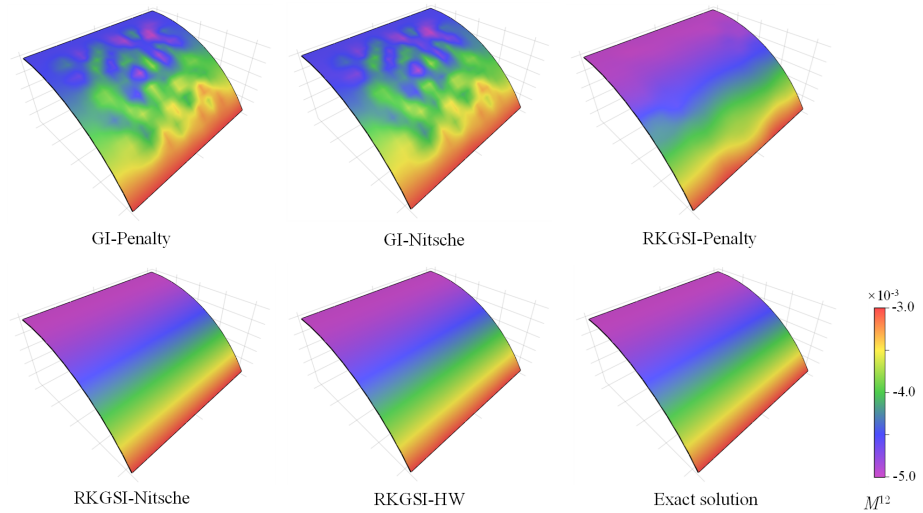


Figure 4: Contour plots of  $M^{12}$  for curved shell patch test.

382 Young's modulus  $E = 4.32 \times 10^8$  and Poisson's ratio  $\nu = 0.0$ . The entire roof  
383 is subjected to an uniform body force of  $b_z = -90$ , with the straight edges  
384 remaining free and the the curved edges are enforced by  $v_x = v_z = 0$ .

385 Due to the symmetry, only a quadrant of the model is considered for meshfree  
386 analysis, which is discretized by the  $11 \times 16$ ,  $13 \times 20$ ,  $17 \times 24$  and  $19 \times 28$  meshfree  
387 nodes, as listed in Fig. 6. The comparison of the displacement in  $z$ -direction at  
388 node  $A$ ,  $v_{A3}$ , is used as the investigated quantity, with the reference value  $0.3024$   
389 given by [35]  $0.3006$  given by [34]. Firstly, Fig. 7 presents a sensitivity study  
390 for the artificial parameters of  $\alpha_v$ 's,  $\alpha_w$ 's and  $\alpha_\theta$ 's in the RKGSI meshfree  
391 formulations with Nitsche's method and penalty method, where all of the  
392 parameters are scaled by the support size as,  $\alpha_{v\alpha} = s^{-1}\bar{\alpha}_v$ ,  $\alpha_{w3} = s^{-3}\bar{\alpha}_w$  and  
393  $\alpha_\theta = s^{-1}\bar{\alpha}_\theta$ . For a better comparison, the result of proposed RKGSI-HW is  
394 also listed in this figure. The results of Fig. 7 revealed, Nitsche's method  
395 observed less artificial sensitivity. However, both the methods cannot trivially  
396 determine the optimal values of the artificial parameters. The optimal artificial

397 parameters from Fig. 7 are adopted for the convergence study in Fig. 8. The  
 398 convergence result showed that the RKGSI get satisfactory results while the  
 399 traditional Gauss methods demonstrated noticeable errors.

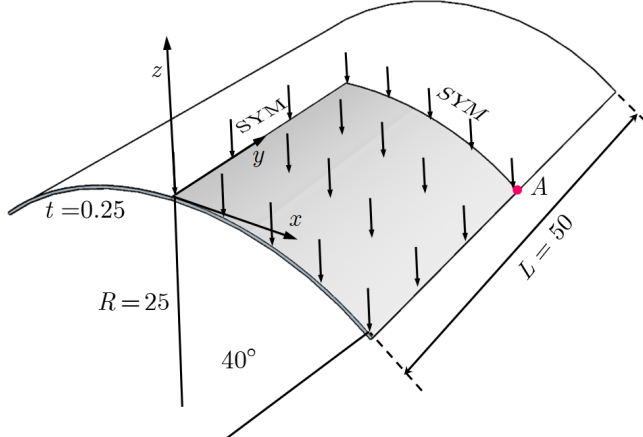


Figure 5: Description of Scordelis-Lo roof problem.

400 *5.3. Pinched Hemispherical shell*

401 Consider the hemispherical shell shown in Fig. 9, which is loaded at four  
 402 points  $P = \pm 2$  at  $90^\circ$  interval at its bottom. The hemispherical shell has an  
 403 radius  $R = 10$ , thickness  $h = 0.04$ , Young's modulus  $E = 6.825 \times 10^7$  and  
 404 Poisson's ratio  $\nu = 0.3$ .

405 Due to symmetry, only quadrant model, where the ~~8 × 8~~,  $16 \times 16$ ,  $24 \times$   
 406 ~~24 and~~ ,  $32 \times 32$  and  $40 \times 40$  meshfree nodes have been discretized as shown in  
 407 Fig. (10), was considered. The quantity under investigation for convergence  
 408 is the displacement at ~~x-direction x-direction~~ on point A,  $v_{A1} = 0.094$  [35].  
 409 Fig. 11 displays the corresponding convergence results, indicating the RKGSI  
 410 scheme performed significantly better compared to the GI meshfree formulation.  
 411 Meanwhile, the efficiency comparison for this problem is also shown in Fig.  
 412 12, in which the CPU time for assembly and calculation of shape functions  
 413 are considered. Fig. 12(a) indicates that the RKGSI scheme observed high  
 414 efficiency in assembly. This is due to the variational inconsistent Gauss meshfree  
 415 formulation which require more Gaussian points to get satisfactory results. Fig.  
 416 12(b) lists the CPU time spent on enforcing essential boundary conditions for  
 417 the penalty method, Nitsche's method and proposed HW method. The results  
 418 highlighted that the proposed HW method consumed comparable CPU time  
 419 in assembly compared to Nitsche's method. However, less time was spent to  
 420 calculate the shape functions. Since both the HW method and penalty method  
 421 were developed considering the shape functions first order derivatives. For this  
 422 reason, both the methods shared an almost identical time in computing the  
 423 shape functions.

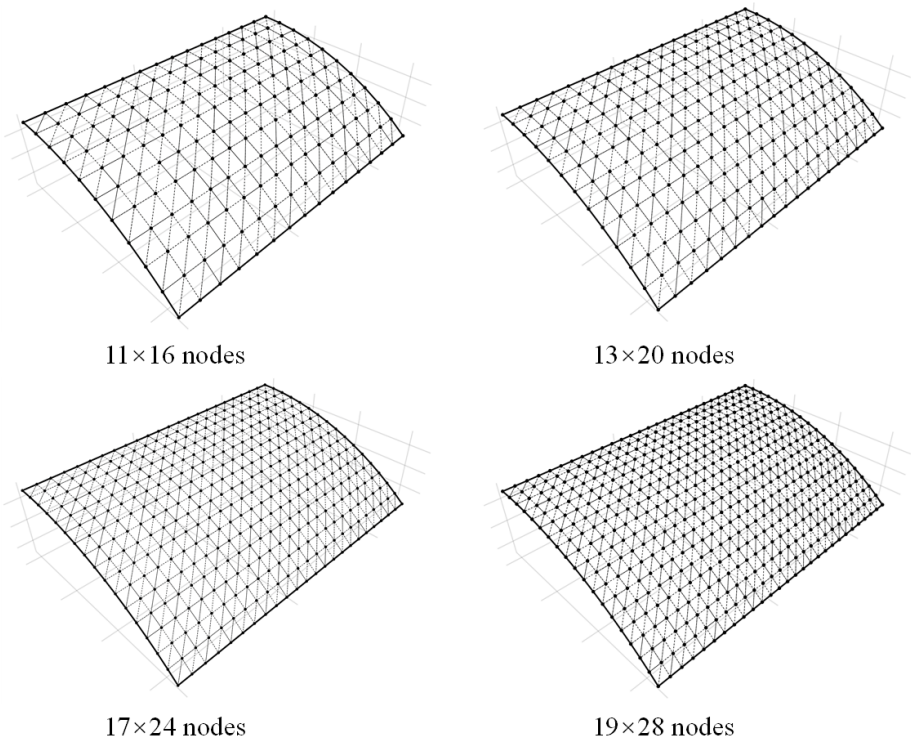


Figure 6: Meshfree discretizations for Scordelis-Lo roof problem.

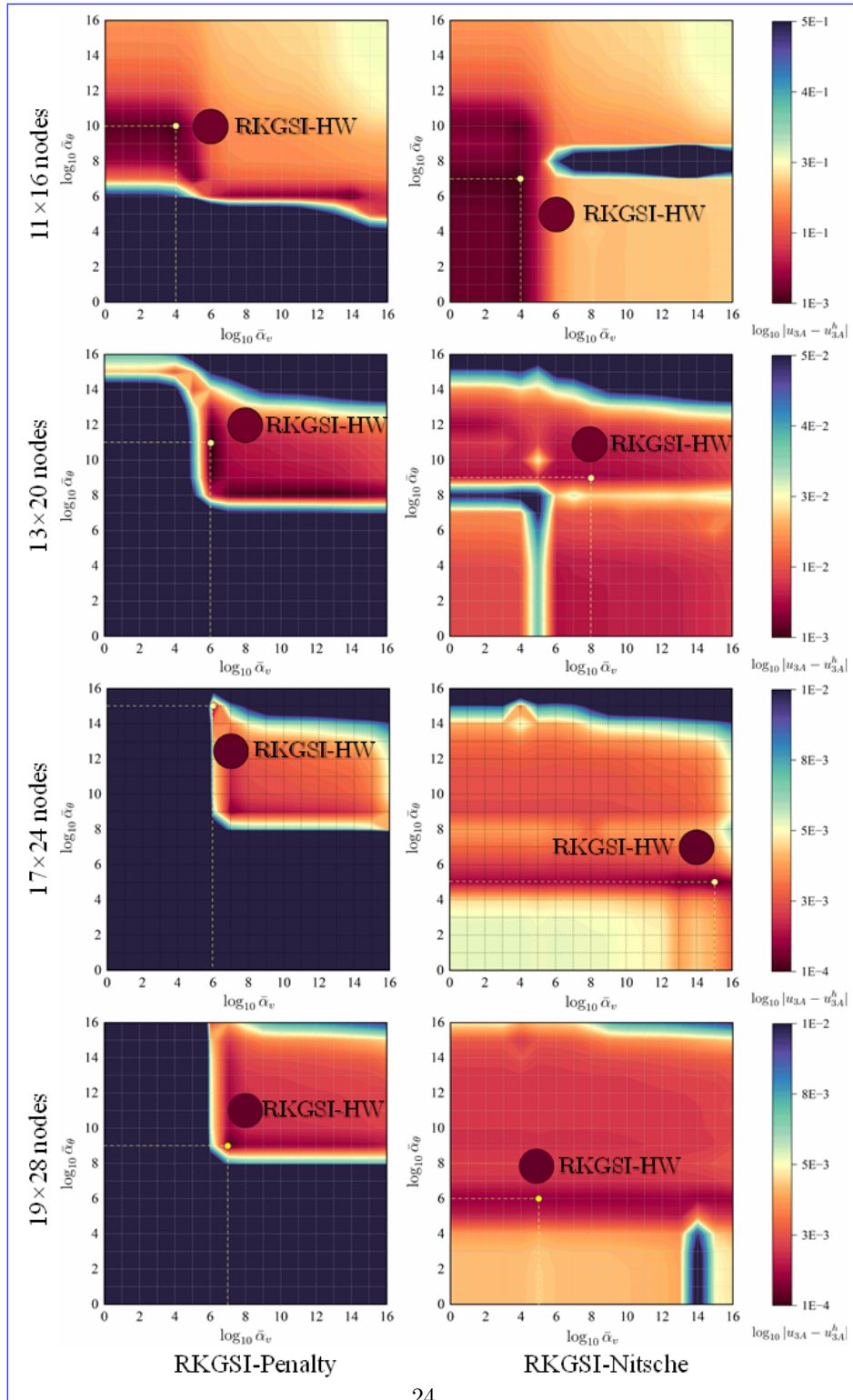


Figure 7: Sensitivity comparison of  $\alpha_v$  and  $\alpha_\theta$  for Scordelis-Lo problem.

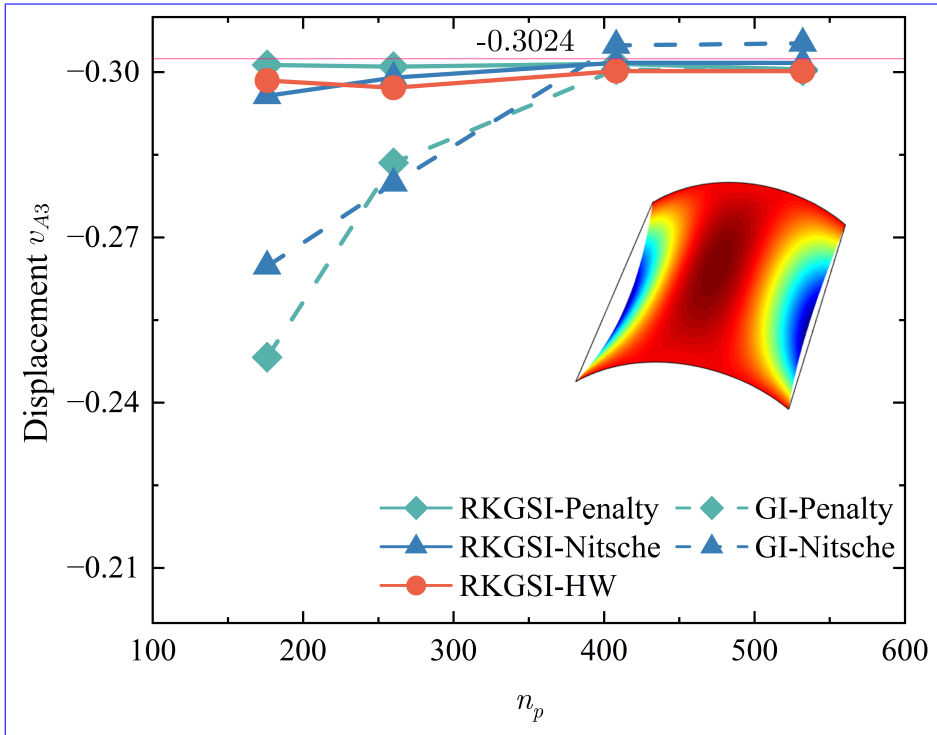


Figure 8: Displacement convergence for Scordelis-Lo roof problem.

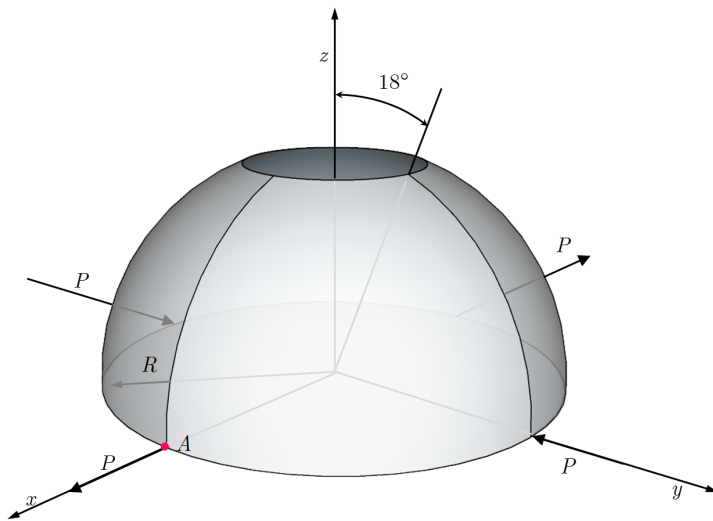


Figure 9: Description of pinched hemispherical shell problem.

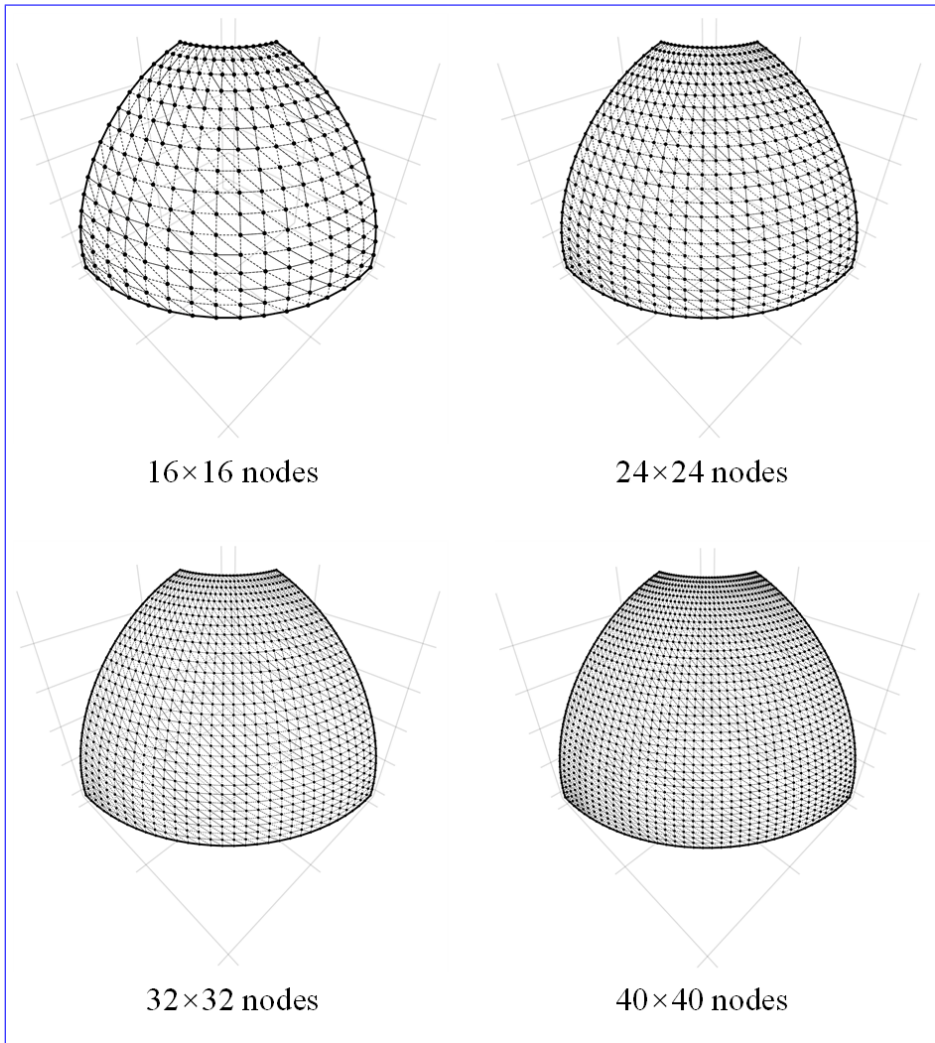


Figure 10: [Meshfree discretizations for pinched hemispherical shell problem.](#)

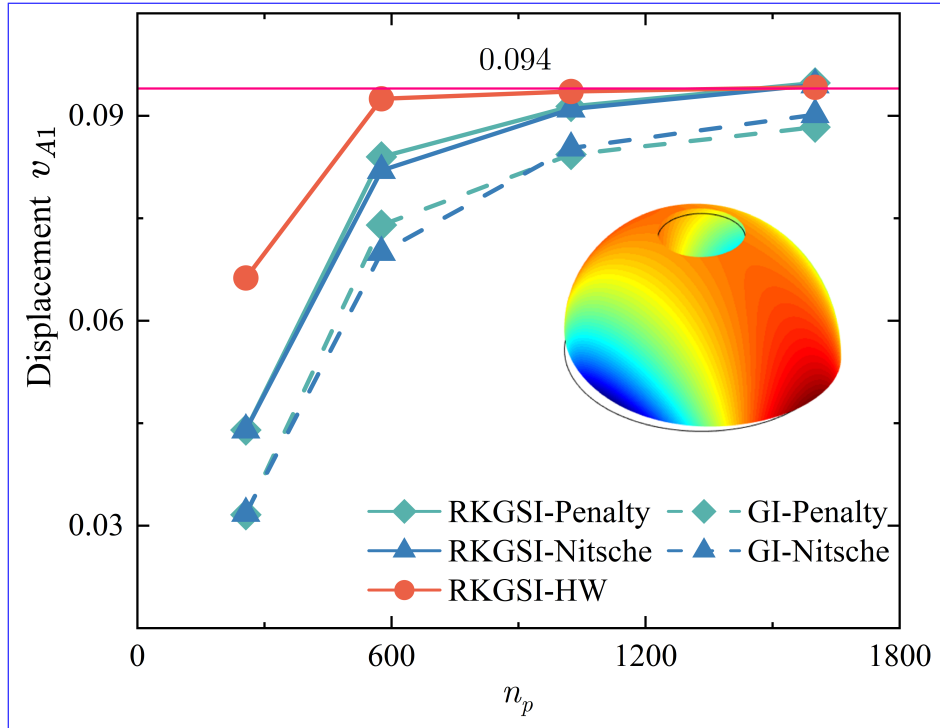


Figure 11: Displacement convergence for pinched hemispherical shell problem.

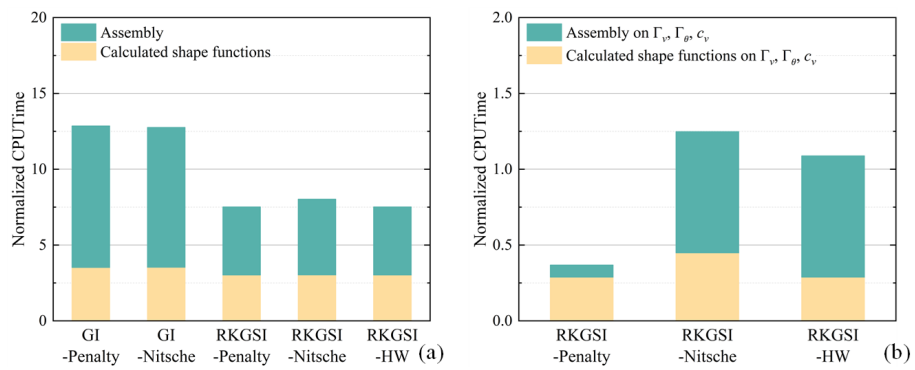


Figure 12: efficiency comparison for pinched hemispherical shell problem: (a) Whole domain; (b) Essential boundaries

424    **6. Conclusion**

425    In this study, an efficient and quasi-consistent meshfree thin shell formu-  
426    lation was presented to naturally enforce the essential boundary conditions.  
427    Mixed formulation with the Hu-Washizu principle weak form is adopted, where  
428    the traditional meshfree shape functions discretized the displacement, and the  
429    strains and stresses were expressed by the reproducing kernel smoothed gradi-  
430    ents and the covariant smoothed gradients, respectively. The smoothed gradient  
431    naturally embedded the first second-order integration constraints and has  
432    a quasi variational consistency for the curved models in each integration cell.  
433    Owing to the Hu-Washizu variational principle, the essential boundary condi-  
434    tion enforcement has a similar form with the conventional Nitsche's method;  
435    both have consistent and stabilized terms. The costly high order derivatives  
436    in the Nitsche's consistent term have been replaced by the smoothed gradients,  
437    which improved the computational speed due to the reproducing kernel gradient  
438    smoothing framework. Furthermore, the stabilized term naturally existed in the  
439    Hu-Washizu weak form, and the artificial parameter needed in Nitsche's stabi-  
440    lized term has vanished, which can automatically maintain the coercivity for  
441    the stiffness matrix. Based on general reproducing kernel gradient smoothing  
442    framework, the proposed methodology can be trivially extended to high order  
443    basis meshfree formulation. The numerical results demonstrated that the pro-  
444    posed Hu-Washizu quasi-consistent meshfree thin shell formulation showed ex-  
445    cellent accuracy, efficiency, and stability.

<sup>446</sup>      **Acknowledgment**

<sup>447</sup>      The support of this work by the National Natural Science Foundation of  
<sup>448</sup> China (12102138, 52350410467) and the Natural Science Foundation of Fujian  
<sup>449</sup> Province of China (2023J01108, 2022J05056) is gratefully acknowledged.

450    **Appendix A. Green's theorems for in-plane vector**

451    This Appendix discusses two kinds of Green's theorems used for the development  
 452    of the proposed meshfree method. For an arbitrary vectors  $v^\alpha$  and a  
 453    scalar function  $f$ , with Green's theorem for in-plane vector, the first Green's  
 454    theorem is listed as follows [31]:

$$\begin{aligned} \int_{\Omega} f_{,\alpha} v^\alpha d\Omega &= \int_{\Gamma} f v^\alpha n_\alpha d\Gamma - \int_{\Omega} f(v_{,\alpha}^\alpha + \Gamma_{\beta\alpha}^\beta v^\alpha) d\Omega \\ &= \int_{\Gamma} f v^\alpha n_\alpha d\Gamma - \int_{\Omega} f v^\alpha|_\alpha d\Omega \end{aligned} \quad (\text{A.1})$$

455    where  $\Gamma_{\alpha\beta}^\gamma = \mathbf{a}_{\alpha,\beta} \cdot \mathbf{a}^\gamma$  denotes the Christoffel symbol of the second kind.  $v^\alpha|_\alpha$   
 456    can be represented as the in-plane covariant derivative of the vector  $v^\alpha$ :

$$v^\alpha|_\alpha = v_{,\alpha}^\alpha + \Gamma_{\beta\alpha}^\beta v^\alpha \quad (\text{A.2})$$

457    The second Green's theorem is established with a mixed form of second  
 458    order derivative. Let  $A^{\alpha\beta}$  can be an arbitrary symmetric second order tensor,  
 459    the Green's theorem yields [31]:

$$\begin{aligned} \int_{\Omega} f_{,\alpha}|_\beta A^{\alpha\beta} d\Omega &= \int_{\Gamma} f_{,\gamma} n^\gamma A^{\alpha\beta} n_\alpha n_\beta d\Gamma - \int_{\Gamma} f(A^{\alpha\beta} s_\alpha n_\beta)_{,\gamma} s^\gamma d\Gamma + [[f A^{\alpha\beta} s_\alpha n_\beta]]_{\mathbf{x}\in C} \\ &\quad - \int_{\Gamma} f(A_{,\beta}^{\alpha\beta} n_\alpha + \Gamma_{\alpha\beta}^\gamma A^{\alpha\beta} n_\gamma + \Gamma_{\gamma\beta}^\gamma A^{\alpha\beta} n_\alpha) d\Gamma \\ &\quad + \int_{\Omega} f \left( \begin{array}{l} \Gamma_{\alpha\beta,\gamma}^\gamma A^{\alpha\beta} + \Gamma_{\alpha\beta}^\gamma A^{\alpha\beta} + \Gamma_{\eta\gamma}^\eta \Gamma_{\alpha\beta}^\gamma A^{\alpha\beta} \\ + A_{,\alpha\beta}^{\alpha\beta} + \Gamma_{\gamma\beta,\alpha}^\gamma A^{\alpha\beta} + 2\Gamma_{\gamma\alpha}^\gamma A_{,\beta}^{\alpha\beta} + \Gamma_{\gamma\alpha}^\gamma \Gamma_{\eta\beta}^\eta A^{\alpha\beta} \end{array} \right) d\Omega \\ &= \int_{\Gamma} f_{,\gamma} n^\gamma A^{\alpha\beta} n_\alpha n_\beta d\Gamma - \int_{\Gamma} f(A^{\alpha\beta} s_\alpha n_\beta)_{,\gamma} s^\gamma d\Gamma + [[f A^{\alpha\beta} s_\alpha n_\beta]]_{\mathbf{x}\in C} \\ &\quad - \int_{\Gamma} f A^{\alpha\beta}|_\beta n_\alpha d\Gamma + \int_{\Omega} f A^{\alpha\beta}|_\alpha n_\beta d\Omega \end{aligned} \quad (\text{A.3})$$

460    with

$$A^{\alpha\beta}|_\beta = A_{,\beta}^{\alpha\beta} + \Gamma_{\beta\gamma}^\alpha A^{\beta\gamma} + \Gamma_{\gamma\beta}^\alpha A^{\alpha\beta} \quad (\text{A.4})$$

$$\begin{aligned} A^{\alpha\beta}|_{\alpha\beta} &= \Gamma_{\alpha\beta,\gamma}^\gamma A^{\alpha\beta} + \Gamma_{\alpha\beta}^\gamma A^{\alpha\beta} + \Gamma_{\eta\gamma}^\eta \Gamma_{\alpha\beta}^\gamma A^{\alpha\beta} \\ &\quad + A_{,\alpha\beta}^{\alpha\beta} + \Gamma_{\gamma\beta,\alpha}^\gamma A^{\alpha\beta} + 2\Gamma_{\gamma\alpha}^\gamma A_{,\beta}^{\alpha\beta} + \Gamma_{\gamma\alpha}^\gamma \Gamma_{\eta\beta}^\eta A^{\alpha\beta} \end{aligned} \quad (\text{A.5})$$

462    For the sake of brevity, the notion of covariant derivative is extended to a  
 463    scalar function as:

$$f|_\alpha = f_{,\alpha} + \Gamma_{\beta\alpha}^\beta f \quad (\text{A.6})$$

$$f|_\beta n_\alpha = f_{,\beta} n_\alpha + \Gamma_{\alpha\beta}^\gamma f n_\gamma + \Gamma_{\gamma\beta}^\gamma f n_\alpha \quad (\text{A.7})$$

$$\begin{aligned} f|_{\alpha\beta} &= \Gamma_{\alpha\beta,\gamma}^\gamma f + \Gamma_{\alpha\beta}^\gamma f_{,\gamma} + \Gamma_{\eta\gamma}^\eta \Gamma_{\alpha\beta}^\gamma f \\ &\quad + f_{,\alpha\beta} + \Gamma_{\gamma\beta,\alpha}^\gamma f + 2\Gamma_{\gamma\alpha}^\gamma f_{,\beta} + \Gamma_{\gamma\alpha}^\gamma \Gamma_{\eta\beta}^\eta f \end{aligned} \quad (\text{A.8})$$

<sup>466</sup> **Appendix B. Derivations for stiffness metrics and force vectors**

<sup>467</sup> This Appendix details the derivations of stiffness matrices and force vectors  
<sup>468</sup> in Eqs. (53)-(55), where the relationships of Eqs. (40), (41), (44) and (46) are  
<sup>469</sup> used herein. Firstly, the membrane strain terms are considered as follows:

$$\begin{aligned}
 & \sum_{C=1}^{n_e} \int_{\Omega_C} \delta \tilde{\varepsilon}_{\alpha\beta}^h h C^{\alpha\beta\gamma\eta} \tilde{\varepsilon}_{\gamma\eta}^h d\Omega \\
 &= \sum_{C=1}^{n_e} \sum_{I,J=1}^{n_p} \delta \mathbf{d}_I \cdot \underbrace{\int_{\Omega_C} \tilde{\varepsilon}_{\alpha\beta I} h C^{\alpha\beta\gamma\eta} \mathbf{a}_\gamma \mathbf{q}^T d\Omega \mathbf{G}^{-1} \bar{\mathbf{g}}_{\eta J} \cdot \mathbf{d}_J}_{\tilde{\mathbf{g}}_I^{\eta T}} \\
 &= \sum_{C=1}^{n_e} \sum_{I,J=1}^{n_p} \delta \mathbf{d}_I \cdot \int_{\Gamma_C \cap \Gamma_v} \Psi_J \underbrace{\mathbf{q}^T \mathbf{G}^{-1} \tilde{\mathbf{g}}_I^\alpha n_\alpha}_{\tilde{\mathbf{T}}_{NI}} d\Gamma \cdot \mathbf{d}_J \\
 &= \sum_{I,J=1}^{n_p} \delta \mathbf{d}_I \cdot \int_{\Gamma_v} \tilde{\mathbf{T}}_{NI} \Psi_J d\Gamma \cdot \mathbf{d}_J
 \end{aligned} \tag{B.1}$$

<sup>470</sup> with

$$\tilde{\mathbf{g}}_I^\alpha = \mathbf{q} \mathbf{a}_\beta h C^{\alpha\beta\gamma\eta} \tilde{\varepsilon}_{\alpha\beta\gamma\eta} \tag{B.2}$$

<sup>471</sup>

$$\tilde{\mathbf{T}}_{NI} = \mathbf{q}^T \mathbf{G}^{-1} \tilde{\mathbf{g}}_I^\alpha n_\alpha \tag{B.3}$$

<sup>472</sup> Following this path, the bending strain terms can be reorganized by:

$$\begin{aligned}
 & \sum_{C=1}^{n_e} \int_{\Omega_C} \delta \tilde{\kappa}_{\alpha\beta}^h \frac{h^3}{12} C^{\alpha\beta\gamma\eta} \bar{\kappa}_{\gamma\eta}^h d\Omega \\
 &= \sum_{C=1}^{n_e} \sum_{I,J=1}^{n_p} \delta \mathbf{d}_I \cdot \underbrace{\int_{\Omega_C} \tilde{\kappa}_{\alpha\beta I} \frac{h^3}{12} C^{\alpha\beta\gamma\eta} \mathbf{a}_3 \mathbf{q}^T d\Omega \mathbf{G}^{-1} \bar{\mathbf{g}}_{\gamma\eta J} \cdot \mathbf{d}_J}_{\tilde{\mathbf{g}}_I^{\gamma\eta T}} \\
 &= \sum_{C=1}^{n_e} \sum_{I,J=1}^{n_p} \delta \mathbf{d}_I \cdot \left( \begin{array}{l} \int_{\Gamma_C \cap \Gamma_\theta} \underbrace{\mathbf{q}^T \mathbf{G}^{-1} \tilde{\mathbf{g}}_I^{\alpha\beta} n_\alpha n_\beta}_{\tilde{\mathbf{M}}_{nnI}} n^\gamma \Psi_{J,\gamma} d\Gamma \\ - \int_{\Gamma_C \cap \Gamma_v} \underbrace{(\mathbf{q}_{|\beta}^T \mathbf{G}^{-1} \tilde{\mathbf{g}}_I^{\alpha\beta} n_\alpha + (\mathbf{q}^T \mathbf{G}^{-1} \tilde{\mathbf{g}}_I^{\alpha\beta} s_\alpha n_\beta)_{,\gamma} s^\gamma)}_{\tilde{\mathbf{T}}_{MI}} \Psi_{J,\gamma} d\Gamma \\ + [[\underbrace{\mathbf{q}^T \mathbf{G}^{-1} \tilde{\mathbf{g}}_I^{\alpha\beta} s_\alpha n_\beta}_{\tilde{\mathbf{P}}_I \mathbf{a}_3} \Psi_J]]_{\mathbf{x} \in C_C \cap C_v} \end{array} \right) \cdot \mathbf{d}_J \\
 &= \sum_{I,J=1}^{n_p} \delta \mathbf{d}_I \cdot \left( \int_{\Gamma_\theta} \tilde{\mathbf{M}}_{nnI} n^\gamma \Psi_{J,\gamma} d\Gamma - \int_{\Gamma_v} \tilde{\mathbf{T}}_{MI} \Psi_{J,\gamma} d\Gamma + [[\tilde{\mathbf{P}}_I \Psi_J]]_{\mathbf{x} \in C_v} \right)
 \end{aligned} \tag{B.4}$$

<sup>473</sup> with

$$\tilde{\mathbf{g}}_I^{\alpha\beta} = \int_{\Omega_C} \mathbf{q} \frac{h^3}{12} C^{\alpha\beta\gamma\eta} \mathbf{a}_3 \tilde{\kappa}_{\underline{\alpha}\underline{\beta}\underline{I}\underline{\gamma}\underline{\eta}\underline{I}} d\Omega \quad (\text{B.5})$$

<sup>474</sup>

$$\begin{cases} \tilde{M}_{nnI} = \mathbf{q}^T \mathbf{G}^{-1} \tilde{\mathbf{g}}_I^{\alpha\beta} n_\alpha n_\beta \\ \tilde{T}_{MI} = \mathbf{q}_{|\beta}^T \mathbf{G}^{-1} \tilde{\mathbf{g}}_I^{\alpha\beta} n_\alpha + (\mathbf{q}^T \mathbf{G}^{-1} \tilde{\mathbf{g}}_I^{\alpha\beta} s_\alpha n_\beta)_{,\gamma} s^\gamma \\ \tilde{P}_I = \mathbf{q}^T \mathbf{G}^{-1} \tilde{\mathbf{g}}_I^{\alpha\beta} s_\alpha n_\beta \cdot \mathbf{a}_3 \end{cases} \quad (\text{B.6})$$

475 **References**

- 476 [1] L. H. Donnell, Beams, Plates and Shells, McGraw-Hill, 1976.
- 477 [2] T. J. Hughes, The Finite Element Method: Linear Static and Dynamic  
478 Finite Element Analysis, Dover Publications, Mineola, New York, 2000.
- 479 [3] T. Belytschko, Y. Y. Lu, L. Gu, Element-free Galerkin methods, Interna-  
480 tional Journal for Numerical Methods in Engineering 37 (1994) 229–256.
- 481 [4] W. K. Liu, S. Jun, Y. F. Zhang, Reproducing kernel particle methods,  
482 International Journal for Numerical Methods in Fluids 20 (1995) 1081–  
483 1106.
- 484 [5] J. S. Chen, M. Hillman, S. W. Chi, Meshfree methods: Progress made after  
485 20 Years, Journal of Engineering Mechanics 143 (2017) 04017001.
- 486 [6] P. Krysl, T. Belytschko, Analysis of thin shells by the Element-Free  
487 Galerkin method, International Journal of Solids and Structures 33 (1996)  
488 3057–3080.
- 489 [7] G. R. Liu, Meshfree Methods: Moving Beyond the Finite Element Method,  
490 Second Edition, Crc Press, 2009.
- 491 [8] X. Zhang, K. Z. Song, M. W. Lu, X. Liu, Meshless methods based on  
492 collocation with radial basis functions, Computational Mechanics 26 (2000)  
493 333–343.
- 494 [9] D. Millán, A. Rosolen, M. Arroyo, Thin shell analysis from scattered points  
495 with maximum-entropy approximants, International Journal for Numerical  
496 Methods in Engineering 85 (2011) 723–751.
- 497 [10] L. Wang, M. Hu, Z. Zhong, F. Yang, Stabilized Lagrange Interpolation  
498 Collocation Method: A meshfree method incorporating the advantages of  
499 finite element method, Computer Methods in Applied Mechanics and En-  
500 gineering 404 (2023) 115780.
- 501 [11] P. Suchde, T. Jacquemin, O. Davydov, Point Cloud Generation for Mesh-  
502 free Methods: An Overview, Archives of Computational Methods in Engi-  
503 neering 30 (2022) 889–915.
- 504 [12] L. Deng, D. Wang, An accuracy analysis framework for meshfree collocation  
505 methods with particular emphasis on boundary effects, Computer Methods in  
506 Applied Mechanics and Engineering 404 (2023) 115782.
- 507 [13] J. Wang, M. Hillman, Upwind reproducing kernel collocation method for  
508 convection-dominated problems, Computer Methods in Applied Mechanics  
509 and Engineering 420 (2024) 116711.

- 510 [14] S. Fernández-Méndez, A. Huerta, Imposing essential boundary conditions  
 511 in mesh-free methods, Computer Methods in Applied Mechanics and En-  
 512 gineering 193 (2004) 1257–1275.
- 513 [15] X. Li, Error estimates for the moving least-square approximation and the  
 514 element-free Galerkin method in n-dimensional spaces, Applied Numerical  
 515 Mathematics 99 (2016) 77–97.
- 516 [16] J. Wu, D. Wang, An accuracy analysis of Galerkin meshfree methods ac-  
 517 counting for numerical integration, Computer Methods in Applied Mechan-  
 518 ics and Engineering 375 (2021) 113631.
- 519 [17] J. S. Chen, H. P. Wang, New boundary condition treatments in meshfree  
 520 computation of contact problems, Computer Methods in Applied Mechan-  
 521 ics and Engineering 187 (2000) 441–468.
- 522 [18] D. Liu, Y. M. Cheng, The interpolating element-free Galerkin (IEFG)  
 523 method for three-dimensional potential problems, Engineering Analysis  
 524 with Boundary Elements 108 (2019) 115–123.
- 525 [19] V. Ivannikov, C. Tiago, P. M. Pimenta, On the boundary conditions of the  
 526 geometrically nonlinear Kirchhoff–Love shell theory, International Journal  
 527 of Solids and Structures 51 (2014) 3101–3112.
- 528 [20] Y. Y. Lu, T. Belytschko, L. Gu, A new implementation of the element free  
 529 Galerkin method, Computer Methods in Applied Mechanics and Engineer-  
 530 ing 113 (1994) 397–414.
- 531 [21] T. Zhu, S. N. Atluri, A modified collocation method and a penalty formu-  
 532 lation for enforcing the essential boundary conditions in the element free  
 533 Galerkin method, Computational Mechanics 21 (1998) 211–222.
- 534 [22] S. Skatulla, C. Sansour, Essential boundary conditions in meshfree methods  
 535 via a modified variational principle: Applications to shell computations,  
 536 Computer Assisted Mechanics and Engineering Sciences 15 (2008) 123–142.
- 537 [23] J. S. Chen, C. T. Wu, S. Yoon, Y. You, A stabilized conforming nodal  
 538 integration for Galerkin mesh-free methods, International Journal for Nu-  
 539 matical Methods in Engineering 50 (2001) 435–466.
- 540 [24] J. S. Chen, M. Hillman, M. Rüter, An arbitrary order variationally consis-  
 541 tent integration for Galerkin meshfree methods, International Journal for  
 542 Numerical Methods in Engineering 95 (2013) 387–418.
- 543 [25] Q. Duan, X. Li, H. Zhang, T. Belytschko, Second-order accurate derivatives  
 544 and integration schemes for meshfree methods, International Journal for  
 545 Numerical Methods in Engineering 92 (2012) 399–424.

- 546 [26] D. Wang, J. Wu, An inherently consistent reproducing kernel gradient  
 547 smoothing framework toward efficient Galerkin meshfree formulation with  
 548 explicit quadrature, Computer Methods in Applied Mechanics and Engi-  
 549 neering 349 (2019) 628–672.
- 550 [27] J. Wang, X. Ren, A consistent projection integration for Galerkin meshfree  
 551 methods, Computer Methods in Applied Mechanics and Engineering 414  
 552 (2023) 116143.
- 553 [28] J. Wu, X. Wu, Y. Zhao, D. Wang, A consistent and efficient method for  
 554 imposing meshfree essential boundary conditions via hellinger-reissner vari-  
 555 ational principle., Chinese Journal of Theoretical and Applied Mechanics  
 556 54 (2022) 3283–3296.
- 557 [29] J. Wu, X. Wu, Y. Zhao, D. Wang, A rotation-free Hellinger-Reissner mesh-  
 558 free thin plate formulation naturally accommodating essential boundary  
 559 conditions, Engineering Analysis with Boundary Elements 154 (2023) 122–  
 560 140.
- 561 [30] H. Dah-wei, A method for establishing generalized variational principle,  
 562 Applied Mathematics and Mechanics 6 (1985) 501–509.
- 563 [31] J. Benzaken, J. A. Evans, S. F. McCormick, R. Tamstorf, Nitsche's method  
 564 for linear Kirchhoff–Love shells: Formulation, error analysis, and verifica-  
 565 tion, Computer Methods in Applied Mechanics and Engineering 374 (2021)  
 566 113544.
- 567 [32] H. Dah-wei, A method for establishing generalized variational principle,  
 568 Applied Mathematics and Mechanics 6 (1985) 501–509.
- 569 [33] H. Du, J. Wu, D. Wang, J. Chen, A unified reproducing kernel gradient  
 570 smoothing Galerkin meshfree approach to strain gradient elasticity, Com-  
 571 putational Mechanics 70 (2022) 73–100.
- 572 [34] J. Kiendl, K. U. Bletzinger, J. Linhard, R. Wüchner, Isogeometric shell  
 573 analysis with Kirchhoff–Love elements, Computer Methods in Applied  
 574 Mechanics and Engineering 198 (2009) 3902–3914.
- 575 [35] R. H. MacNeal, R. L. Harder, A proposed standard set of problems to test  
 576 finite element accuracy, Finite Elements in Analysis and Design 1 (1985)  
 577 3–20.